UNIVERSITY OF CATANIA

DEPARTMENT OF DRUG SCIENCES

BIOCHEMISTRY SECTION

PhD in BASIC AND APPLIED BIOMEDICAL SCIENCES
Coordinator: Prof. Massimo Libra

MARIA DOMENICA DI MAURO

BIOMOLECULES FROM OLIVE MILL WASTEWATER: COSMECEUTICAL AND NUTRACEUTICAL APPLICATIONS

PhD Degree

SUPERVISOR
Prof. Marcella Renis

ASSISTANT SUPERVISORS
Dr. Nicola D'Antona
Dr. Barbara Tomasello

ACADEMIC YEAR 2017-2018

INDEX

ABSTRACT

Background

Green Chemistry is an emerging approach which aims at achieving sustainability at the molecular level in all industry sectors, by eliminating the use and generation of hazardous substances (Anastas and Warner, 2007; Anastas and Eghbali, 2010) and producing huge amounts of high added value by-products useful in different fields, such as pharmaceutical, nutraceutical, cosmetic and food (Ferri et al., 2016; Routray and Orsat, 2017, Schieber 2017). In this scenario, the project of the present research has been planned. We focused on olive mill wastewater (OMWW), the main by-product of the olive oil extraction process, constituted by vegetable water of the fruit and the water used in different stages of oil extraction. Its composition is strictly dependent on olive cultivar, ripeness of the fruit, processing techniques, climate and storage conditions (Obied et al., 2008). OMWW contain water, sugars and mineral salts other than proteins, polyalcohols, organic acids, oil residues and polyphenols; among these the most abundant being hydroxytyrosol, a biophenol with a lot of beneficial effects on human health, as anticancer activities (Cabrera et al., 1996).

Aims of our research

Due to the importance of olive oil in the economy of Sicily, our group has been trying to evaluate the nutraceutical properties of OMWW and, in particular, of the hydroxytyrosol component. Indeed, the aims of my doctorate project were to evaluate:

1) some possible differences between the chemical composition of two OMWW generated from different Sicilian olive cultivar (Cerasuola and Nocellara etnea);

2) safety and the moisturizing properties of a sugars and minerals enriched fraction (SMEF), obtained from Cerasuola-OMWW, by *in vitro* and *in vivo* studies;

3) the chemotherapeutic activities *in vitro* exhibited by hydroxytyrosol-enriched fraction (H-EF) obtained from Cerasuola-OMWW. As control, we used hydroxytyrosol commercial standard (HTyr).

Results

Chemical analysis of OMWW

Cerasuola-OMWW and Nocellara etnea-OMWW are similar for mildly acidic pH, high levels of COD, sugars, nitrogen and minerals, but total phenolic and flavonoid content is almost double in Cerasuola-OMWW with respect to Nocellara etnea-OMWW.

HPLC analysis evidenced that hydroxytyrosol and tyrosol were the most abundant biophenols present in both OMWW. The chromatograms highlighted a quantitative rather than a qualitative difference in the polyphenolic profiles of Cerasuola-OMWW and Nocellara etnea-OMWW. Both waters were able to quench the DPPH radical, in a dose dependent manner, and had a higher radical scavenging activity than the positive standard hydroxytyrosol, probably due to the synergistic effect of other phenolic compounds present in OMWW.

Storage condition of OMWW affected phenols and flavonoids stability and hydroxytyrosol concentration being both decreased, especially in Nocellara etnea-OMWW, in a temperature- and time-dependent manner, when stored at 4°C and 25°C for 45 days. Conversely, a slight increase was observed in Cerasuola-OMWW samples stored in the same way, probably due to the hydrolysis of oleuropein and verbascoside.

However, no significant changes were observed in total phenolic, flavonoid and hydroxytyrosol content in both OMWW samples when stored at -20°C for 6 months.

Cosmeceutical application of lyophilized SMEF

The lyophilized SMEF obtained from Cerasuola-OMWW was rich in sugars (around 43%) and potassium in accordance with literature data. In contrast, soluble polysaccharides were not identified probably because these compounds were highly diluted in OMWW or were hydrolyzed in their monosaccharide units due to the acidic pH of the sample.

The *in vitro* study performed on MRC-5 cells has evidenced that:

- the lowest concentrations of lyophilized SMEF (0.5% and 1% w/w) did not influence cell viability either after 6 or 24 hours of treatment. Conversely, the highest concentrations (2%, 5% and 10% w/w) determined a drastic decrease of cell viability in a dose- and time-dependent manner;
- the degree of apoptosis and intracellular ROS levels increased, in treated fibroblasts compared to untreated controls, in a dose- and time-dependent way, in particular from 2% concentration to 5% w/w;
- the DNA damage extent increased for the 2% and 5% SMEF treatment only in a concentration-dependent manner; this early SMEF-induced DNA injury may result from the hypertonicity of the culture medium, that increased from 0.278 Osm kg^{-1} for the basic medium up to 0.579 Osm kg^{-1} for the medium supplemented with 5% of the SMEF, or a low DNA repair capability by glucose genetic control as suggested by Pang et al.2012;
- the increase of ROS levels was well correlated to cell viability ($r = 0.9661$, $p = 0.007$), TUNEL+ cells ($r = 0.9945$, $p = 0.005$) and DNA fragmentation ($r = 0.9540$, $p = 0.012$) only at 24 hours as shown by Pearson test;
- the treatment with the highest concentrations of SMEF for 6h induced early alterations of cell morphology as shrunken cytoplasm and numerous blebs and ruffles on the cell surface. These morphological alterations, expression of the compromised cellular redox

status with the involvement of DNA damage, may be produced by the possible formation of inter/intramolecular hydrogen bonds and/or by the presence of pores in the multiple membranes.

Taking into account these data, 1% w/w of lyophilized SMEF was incorporated in an emulsion (F1) to formulate a body cream having a pH value weakly acidic (5.62 ± 0.02), compatible with the skin pH range (4.1-5.8). In addition, the results of ICP-MS analysis evidenced a heavy metals content below limits provided by Italy, German Federal Government and Canada (BfR 2006; Bocca et al., 2014; Health Canada-Santé Canada, 2012).

As obtained by stability studies, F1 emulsion, stored at 25°C±2°C with 60±5% R.H., did not show a significant change over time neither in pH nor in exterior aspect and showed only a minimal browning when stored at 40°C±2°C with 60±5% R.H. for 6 months. In addition, no significant changes in pH, phase separation and/or exterior aspect were observed in F1 samples with respect to base formulation (F0). The *in vivo* study showed that F1 containing lyophilized SMEF (1% w/w) determined an % increase of skin hydration (Group A:122.72%) with respect to F0 (Group B: 57.69%) after 7 days of body cream application and also with respect to day 0. These data are in accordance with the results of other authors who have investigated different cosmetic formulations for their hydration properties (Fujioka et al., 2009; Wanitphakdeedecha et al., 2011).

Nutraceutical application of H-EF

H-EF added at different concentration in astrocytoma cells decreases cell viability, in a dose- and time-dependent manner, induced arrest in G1 phase and inhibited cell migration accordingly (Bassani et al., 2016). These data are in accordance with the observed time-dependent increase in DNA damage and the decrease in p53 and p21 expression, two

proteins considered to be guardians of the genoma. An increase in ROS level with a parallel decrease in GSH level seemed to be involved in the genotoxic effect-EF- induced in astrocytoma cells. In addition, by investigating some possible epigenetic effects exerted by our extract, we observed a modulation of global DNA methylation expressed as hypomethylation at lowest concentration (50 μM) and hypermethylation when the cell treatment was performed at 100 μM. The additional epigenetic parameters we studied, SIRT1 expression and nuclear sirtuins activities, were both decreased.

We observed different dose- and time-dependent effect for hydroxytyrosol (HTyr) 100 μM. The compound did not influence cell viability either after 24 or 48 hours of treatment but induced an arrest in S phase at 24 h and in G1 phase only at 48 h. In addition, it increased p53 expression without inducing any change in p21 expression and, finally, it hypomethylated DNA and increased both SIRT 1 expression and nuclear sirtuins activity.

Conclusion

Our results encourage the use of OMWW from some Sicilian cultivars for the production of both H-EF and SMEF. In view of that, we demonstrated the safe use of SMEF in cosmeceutical field for the first time. Conversely, H-EF showed potentiality for the development of nutraceutical and/or dietary supplements, being potentially helpful in the prevention and/or integrative treatment of lifestyle-associated pathologies such as cancer. Still, considering also the extract capability in modulating oxidative status and epigenetic activity, it could find application in other diseases, as cardiovascular, metabolic and neurodegenerative. However, it is clear that its possible therapeutic use in humans requires additional studies on its action mechanism and synergic effect *in vivo,* other than applications in clinical trials.

PREMISE

Green Chemistry and valorization of food by-products

Green Chemistry, first defined at the beginning of 1990s as the "design of chemical products and processes to reduce or eliminate the use and generation of hazardous substances", is not a new branch of science, but an emerging and different approach which aims at achieving sustainability at the molecular level, finding several applications in all industry sectors (Anastas and Warner, 2007, Anastas and Eghbali, 2010).

Green Chemistry works as an integrated cohesive system of principles or design criteria (Anastas and Eghbali, 2010). The Twelve Principles of Green Chemistry, introduced in 1998 by Paul Anastas and John Warner, are shown in **Figure 1**.

Figure 1. The Twelve Principles of Green Chemistry

The first principle of Green Chemistry states it is better to prevent the formation of waste rather than to clean it up. However, when the production of wastes cannot be avoided, innovative solutions should be considered.

It is well known that food industries are responsible for the production of more than 25 billion ton CO^2- eq. (Schmidt and Merciai, 2014) other than huge amounts of solid and liquid wastes and by-products including fruit pomace, seeds, spent grain powders and liquid effluents (Ferri et al., 2016; Routray and Orsat, 2017). During these recent years, researchers and the industrial community have been attracted by food processing by-products since they contain high added value compounds, as polyphenols, vitamins, minerals and dietary fibers, which can be recovered and find useful applications in pharmaceutical, nutraceutical, cosmetic and food fields (Ferri et al., 2016; Schieber 2017).

Rodrigues et al. (2016) have evaluated the potential application of coffee silverskin extract in cosmetic formulations with antioxidant activity; Denis et al. (2013) have reported the beneficial effects of apple peel polyphenols on oxidative stress and inflammation; Aliakbarian et al. (2012) have demonstrated that polyphenols-enriched extract from olive pomace exerts an antioxidant activity which is able to modulate the response of endothelial cells to oxidative stress, representing a new strategy for the treatment and chemoprevention of endothelial dysfunction and vascular disease.

Literature data certainly report so many examples of recovery of bio-active compounds from different food by-products and their relative applications, but our interest has been focused on the valorization of olive mill wastewater, the main by-product of the olive oil extraction process.

CHAPTER I

INTRODUCTION

1.1 Olive mill wastewater

Olive mill wastewater (OMWW), which is composed of vegetable water of the fruit and the water used in different stages of oil extraction, represent the main by-product of olive oil industry (Roig et al., 2006). Huge amounts of OMWW, ranging from 7 to 30 million m^3, are produced annually in the world. However, the amount of OMWW produced depends on the method used for the olive oil extraction process. Traditional discontinuous pressing process adding a small amount of water, generates small volumes of OMWW (40 to 60 L/100 kg olives); differently from continuous three-phase decanter process producing higher volumes of OMWW (80–120 L/100 kg olives), because of higher amounts of water used in the process (Dermeche et al., 2013).

Figure 2. Olive mill wastewater

OMWW are characterized by a dark color (**Figure 2**), a mildly acidic pH, high electrical conductivity and high organic content (biochemical oxygen demand (BOD) of 35-132 g/L, chemical oxygen demand (COD) of 30-320 g/L) (Dermeche et al., 2013).

OMWW chemical composition is strictly related to different parameters such as olive cultivar, ripeness of the fruit, processing techniques, climate and storage conditions (Dermeche et al., 2013; Obied et al., 2008) but generally OMWW contain water (83-94%), organic matter (4-16%) and mineral salts (0.4-2.5%), potassium being the most abundant, followed by calcium, sodium and magnesium, alongside carbonates and phosphates.

The organic matter is mainly composed of sugars (13-53%), polyphenols (2-15%), proteins (8-16%), polyalcohols (3-10%), organic acids (3-10%) and oil residues (1-14%) (Cabrera et al., 1996).

In addition, concerning the carbohydrates fraction, OMWW contain highly diluted polysaccharides. Galanakis et al. (2010) have reported the sugar compositions of the insoluble and soluble fractions obtained from the alcohol-insoluble residue. The insoluble fraction is rich in rhamnose, glucose, galacturonic acid and xylose and is poor in galactose, arabinose and mannose; whereas the soluble fraction - the most abundant - is composed of galacturonic acid and arabinose, proving the occurrence of pectic polysaccharides.

Regarding the polyphenolic content, phenyl alcohols, phenolic acids, secoiridoids and flavonoids are commonly identified in OMWW (El-Abbassì et al., 2012; He et al., 2012). Structure of major polyphenols present in OMWW is shown in **Figure 3.**

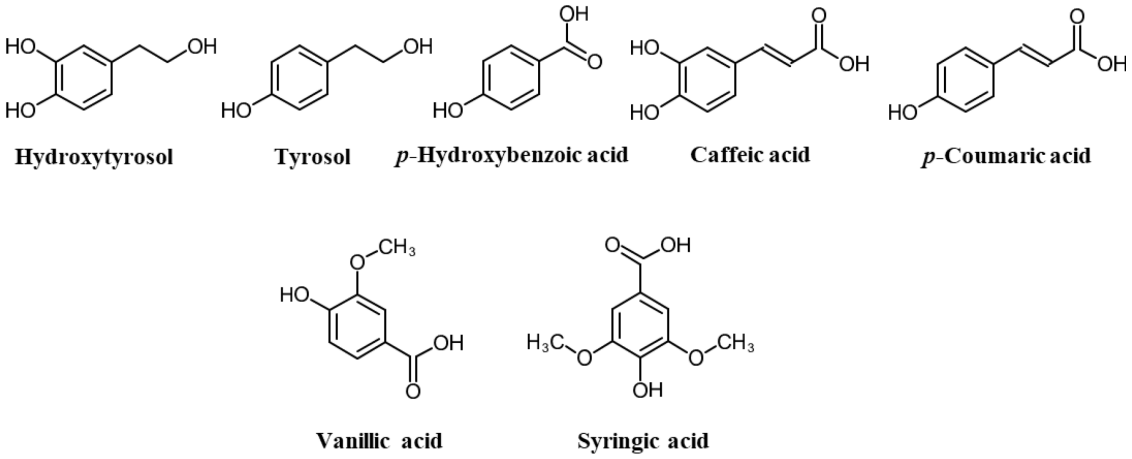

Figure 3. Structure of major polyphenols in OMWW.

Bianco et al., (2003) have evaluated the polyphenolic profile of vegetation waters coming from Canino olives, reporting the presence of hydroxytyrosol, tyrosol, gallic acid, *p*-hydroxybenzoic acid, vanillic acid, caffeic acid, syringic acid, *p*-coumaric acid, ferulic acid and oleuropein. However, as previously reported, it is well known that the qualitative and quantitative phenolic profile of OMWW is strictly related to olive variety and/or to the production process along with storage conditions (Aggoun et al., 2016; D'Antuono et al., 2014; Obied et al., 2008); for instance, El-Abbassì et al. (2012) have observed that OMWW generated from traditional discontinuous press processes have a higher phenolic content than OMWW which is obtained from more modern three-phase centrifugal systems. Although OMWW polyphenolic composition has been investigated in samples coming from Algerian (Azerraj, Sigoise, Chemlal), Australian (Barnea), Greek (Koroneiki, Lianolia and Asprolia) and Italian (Cellina and Coratina) olive cultivars (Aggoun et al., 2016; He et al., 2012; D'Antuono et al., 2014) there are no data about some of the most important Mediterranean productions, such as the Sicilian ones.

For a long time, OMWW have represented a serious economic and environmental issue for the olive oil producers, due to the high organic and inorganic content, responsible for

negative effects on soil microbial populations (Paredes et al., 1987), aquatic ecosystems (Della Greca et al., 2001) and air (Rana et al., 2003).

Several techniques have been employed to recover phenolic compounds from OMWW, including solvent extraction, membrane separation and chromatographic procedures (Alfano et al., 2018; Fava et al., 2017; Zagklis et al., 2015).

1.2 Sugars and minerals for cosmeceutical application

The term cosmeceuticals refers to substances having both cosmetic and therapeutic benefits, being also efficient for treating various dermatologic conditions, nourishing and improving the appearance of the skin, and delivering nutrients which are necessary for healthy skin (Kadam Vaishali et al., 2013).

Literature data have demonstrated that an adequate hydration of the stratum corneum is an effective method to maintain healthy skin (Hoeksema et al., 2013). Indeed, it is well known that the lack/loss of skin water can produce various effects from dryness to more serious conditions such as reduced turgor, thickness and density; in addition, it can accelerate wrinkle formation along with other aging signs, also promoting the onset of irritation, inflammation, itchiness and sensitivity.

Sugars and minerals represent some of the hygroscopic components of natural moisturizing factor (NMF) present inside the corneocytes. These compounds play a crucial role in maintaining hydration, pH and stiffness of stratum corneum. They act as humectants *in vivo*, drawing water up from the dermis to the epidermis as shown in **Figure 4** (Flynn et al., 2001; Rawlings and Harding, 2004; Rodrigues et al., 2015; Verdier-Sévrain and Bonté, 2007).

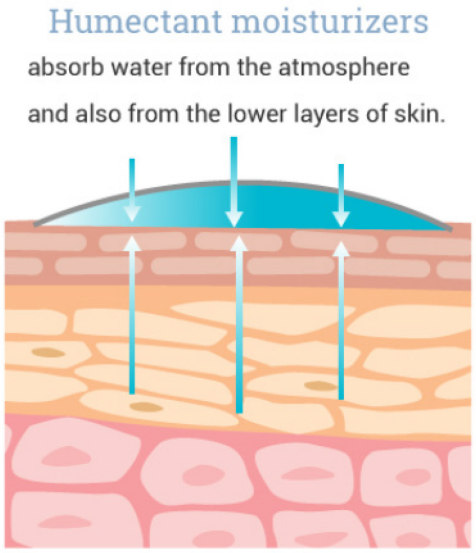

Figure 4. Humectan moisturizers activity

In addition, *in vitro* studies on human keratinocytes have shown the ability of a hypertonic culture medium, sugars containing, to increase the aquaporin-3 mRNA expression, whose protein facilitates water/glycerol transport in the epidermis of normal skin (Sugiyama et al., 2001).

Therefore, sugars and minerals present in OMWW could represent useful cosmeceutical ingredients as suggested by Rodrigues et al., 2015. However, experimental researches about this specific topic are not found in literature.

1.3 Hydroxytyrosol and its biological effects

Hydroxytyrosol, the most abundant biophenol present in OMWW (D'Antuono et al., 2014), is well known for its beneficial effects on human health (Hu et al., 2014).

A body of literature data has evidenced that hydroxytyrosol exerts antioxidant (Grasso et al., 2003), antimicrobial (Zoric et al., 2013), anti-inflammatory (Scoditti ed al., 2014), hypoglycemic (Hamden et al., 2009) and cardioprotective (Tejada et al., 2017) activities.

In particular, Hamden et al. (2009) have evaluated the effect of purified hydroxytyrosol from OMWW on oxidative stress and hyperglycemia in alloxan-induced diabetic rats. The administration of hydroxytyrosol in diabetic rats decreased glucose level in plasma, alongside triglycerides, total-cholesterol and HDL-cholesterol levels in serum; in addition, an increase in renal superoxide dismutase, catalase and glutathione peroxidase activities in liver and kidney was observed.

Several *in vitro* studies have also reported that hydroxytyrosol is able to exert anticancer effects on different breast, colon (Corona et al., 2009; López de las Hazas et al., 2017; Sun et al., 2014), liver, prostate, thyroid (Toteda et al., 2016) and pancreatic (Goldsmith et al., 2018) cancer cell lines. These data are confirmed by some *in vivo* studies performed on male nude BALB/c mice in which tumors were established by the subcutaneous injection of the human cholangiocarcinoma cells (TFK-1) (Li et al., 2014).

1.3.1 Effects on reactive oxygen species in cancer cells

Reactive oxygen species (ROS) are highly reactive radicals, ions or molecules due to the presence of a single unpaired electron in their outermost shell of electrons.

Under physiological conditions, the intracellular stadily maintained levels of ROS act as signaling molecules counteracting some cellular damage to the main macromolecules through non-enzymatic molecules (i.e. glutathione GSH, flavonoids, vitamins A, C and E) or antioxidant enzymes as superoxide dismutases (SOD), catalase, glutathione reductase, glutathione peroxidases and glutathione S-transferases **(Figure 5)** (Liou and Storz , 2010).

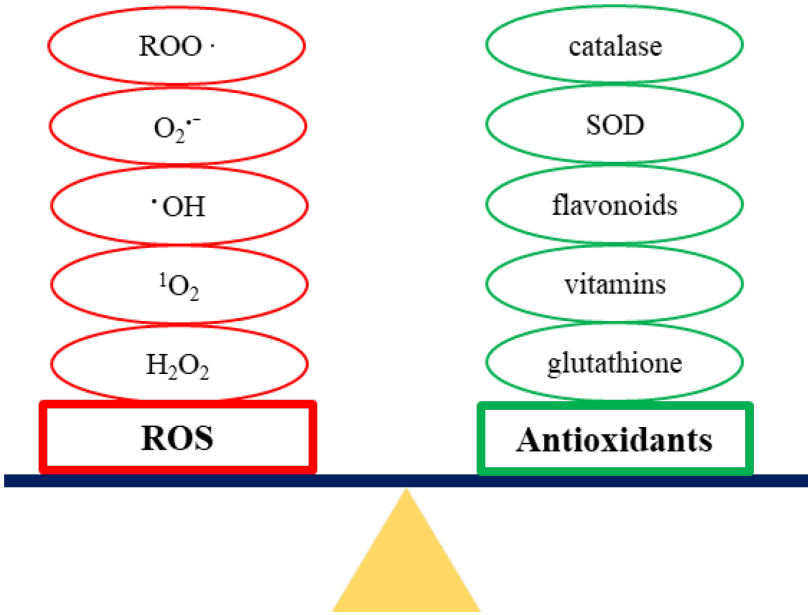

Figure 5. Equilibrium between ROS and antioxidants under physiological conditions.

Increased production of ROS and/or alterations of ROS-scavenging enzymes have long been observed in cancer cells, suggesting an aberrant regulation of redox homeostasis. Metabolic alterations, mitochondrial dysfunction, loss of functional p53, as well as activation of oncogenes, are intrinsic factors responsible for the increased ROS production in cancer cells (Trachootham et al., 2009). High ROS levels may promote tumor formation or progression, leading to cell cycle progression, increase in proliferation and survival signaling, motility, genomic instability and angiogenesis **(Figure 6)** (Liou et al., 2010).

In contrast, a massive increase in intracellular ROS levels can induce cell cycle arrest, senescence or cell death of cancer cells, or a redox adaptation through an overexpression of endogenous antioxidants (**Figures 6 and 7**) (Liou et al., 2010).

The redox adaptation can induce not only the survival of cancer cells, but also the drug resistance as shown in **Figure 7** (Trachootham et al., 2009).

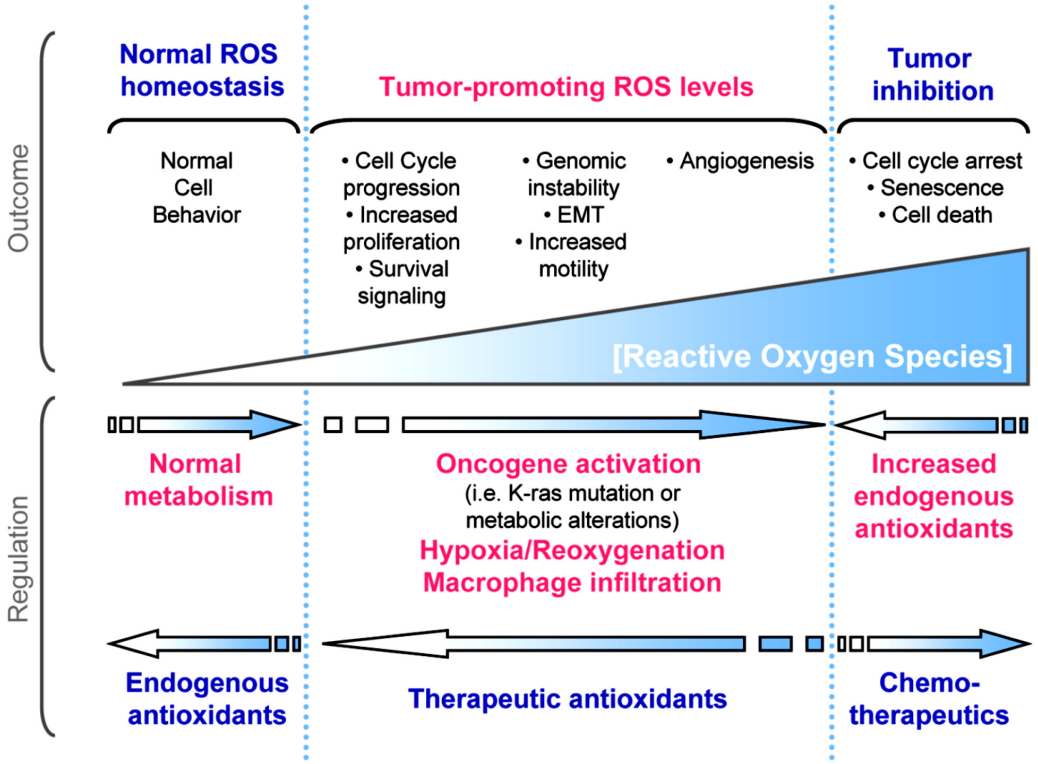

Figure 6. Generation, regulation and effects of cellular ROS (Liou et al., 2010).

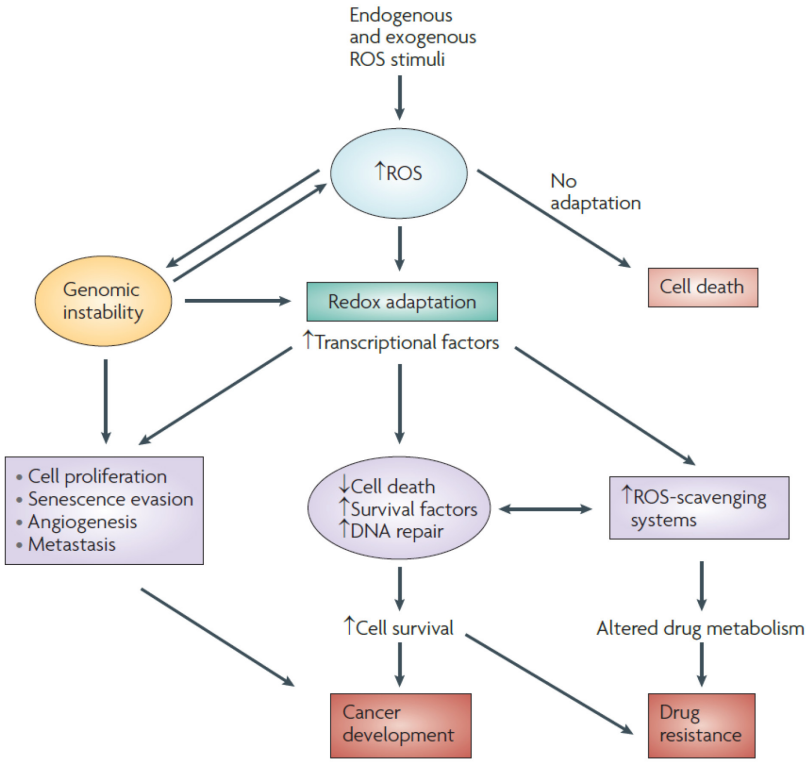

Figure 7. Redox adaptation in cancer cells (Trachootham et al., 2009)

Therefore, a combination of ROS-generating agents with compounds capable of suppressing the cellular antioxidant systems could represent a valid therapeutic approach in cancer treatment.

Bahlis et al. (2002) have already reported the clinical effectiveness of the combinations of arsenic trioxide and ascorbic acid-mediated GSH depletion in the treatment of relapsed or refractory multiple myeloma.

Several studies have highlighted hydroxytyrosol as ROS increasing molecule in different cancer cell lines (Luo et al., 2013; Sun et al., 2014). In particular, Luo et al. (2013) have demonstrated the crucial role exerted by ROS in prostate cancer cells, reporting, in *in vitro* model (PC-3, DU145), the hydroxytyrosol-induced decrease in cell viability and an increase in superoxide production. Similar results have been obtained on colon cancer cells (DLD1) by Sun et al. (2014).

1.3.2 Effects on cell cycle in cancer cells

It is well known that the cell cycle is controlled by numerous mechanisms as regulation of cyclin-dependent kinases (CDK) by cyclins, CDK inhibitors and phosphorylating events (Vermeulen et al., 2003).

CDK are a family of serine/threonine protein kinases which are activated through the binding of cyclins at specific points of the cell cycle as shown in **Figure 8**. The cyclins D bind to CDK4 and to CDK6 and the formed complexes are essential for entry in G1 phase; the cyclin E binds to CDK2 and the complex regulates the progression from G1 into S phase; the cyclin A can bind both CDK2 and CDK1 generating complexes respectively required during S phase or to promote the entry in M phase; the cyclin B forms a complex with CDK1 regulating the mitosis **(Figure 8)**.

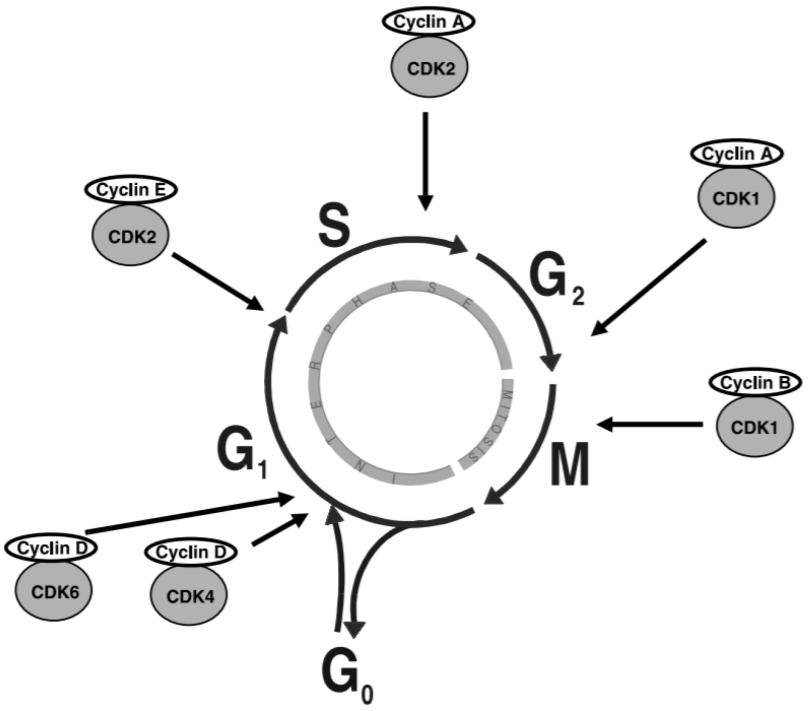

Figure 8. CDK/cyclin complexes: sites of regulatory activity (Vermeulen et al., 2003)

In addition to cyclin binding, CDK activity is also regulated by phosphorylation on conserved threonine and tyrosine residues and by cell cycle inhibitory proteins, called CDK inhibitors (CKI), which bind to CDK alone or to the CDK-cyclin complex.

Two CDK inhibitors families have been discovered: the INK4 family and Cip/Kip family. The INK4 family - including p15, p16, p18 and p19 - specifically inactivates G1 CDK (CDK4 and CDK6), forming stable complexes with the CDK enzyme prior to cyclin binding, thus, preventing the association with cyclin D. The Cip/Kip family - including p21, p27 and p57 - is able to inactivate CDK-cyclin. In particular, p21, a small protein with 165 amino acids - which can be induced by both p53-dependent and p53-independent mechanisms - is able to arrest the cell cycle progression in G1/S and G2/M transitions by inhibiting respectively CDK4,6/cyclin-D and CDK2/cyclin-E (Karimian et al., 2016).

In cancer, cell cycle deregulation occurs through mutation in genes encoding CDK, cyclins, CDK-activating enzymes, CKI, CDK substrates and checkpoint proteins (Sherr 1996).

A body of literature data has shown that hydroxytyrosol effects in different cancer cells are also elicited by inducing an arrest of cell cycle in different phase according with cellular types. In fact, an hydroxytyrsol-induced arrest in G2/M phase has been demonstrated in human colon cancer cells, in different human liver cancer cells (HepG2, Hep3B, SK-HEP-1 and Huh-7) and in pancreatic cancer cells (MIA PaCa-2) (Corona et al., 2009; Goldsmith et al., 2018; Zhao et al., 2014). In contrast, other authors have reported that hydroxytyrosol is able to arrest cell cycle in G1 phase in colon and prostate cancer cells (López de las Hazas et al., 2017; Zubair et al., 2017).

In addition, Zubair et al. (2017) have highlighted that hydroxytyrosol can affect the expression of several cell-cycle-associated proteins in different prostate cancer cell lines (LNCaP and C4-2). In particular, they have shown that hydroxytyrosol decreases the expression of cyclins D1 and E as well as CDK2 and CDK4, while it increases p21 and p27 in both cell lines. Similar results have been reported by Toteda et al. (2016), who have investigated on the expression of cyclin D1 and p21 in terms of mRNA and protein content in thyroid cancer cells (TPC-1, FB-2 and WRO) exposed for 24 h to 324 μM of hydroxytyrosol.

1.3.3 Effects on apoptosis/necrosis in cancer cells

Apoptosis, well known as programmed cell death, plays a crucial role in many physiological processes including cell turnover and embryonic development. However, inappropriate apoptosis is a key factor in many human diseases such as cancer.

Apoptosis is characterized by specific morphological characteristics (Elmore 2007) such as cell shrinkage and chromatin condensation; moreover plasma membrane blebbing occurs followed by separation of cell fragments into apoptotic bodies, containing dense cytoplasm with tightly packed organelles, which are subsequently phagocytosed by macrophages.

The mechanisms of apoptosis are highly complex and involve an energy-dependent cascade of molecular events (**Figure 9**). The extrinsic or death receptor pathway, the intrinsic or mitochondrial pathway and granzyme B pathway converge on the same execution pathway, which is initiated by the cleavage of caspase-3 and results in DNA fragmentation, degradation of cytoskeletal and nuclear proteins, cross-linking of proteins, formation of apoptotic bodies, expression of ligands for phagocytic cell receptors and finally uptake by phagocytic cells. The granzyme A pathway activates a caspase-independent cell death pathway via single stranded DNA damage. Caspase-3, alongside caspase-7, act as "executioner" caspases, cleaving different substrates such as poly (ADP-ribose) polymerase-1 (PARP-1). The cleavage of PARP-1 in two fragments of 89-kD and 24-kD is considered a hallmark of apoptosis (Ganta Vijay Chaitanya et al., 2010).

The control and regulation of apoptotic mitochondrial events occur through Bcl-2 family proteins, including pro-apoptotic (Bcl-10, Bax, Bak) or anti-apoptotic (Bcl-2, Bcl-x, Bcl-XL, Bcl-XS, Bcl-w, BAG) proteins.

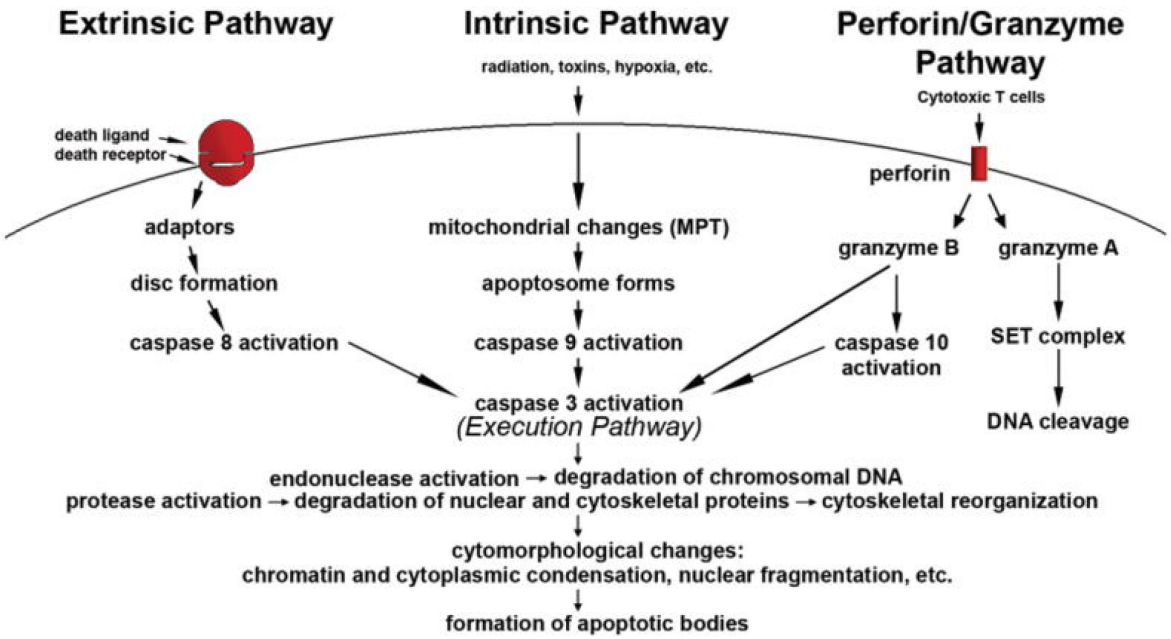

Figure 9. Schematic representation of apoptotic events (Elmore 2007)

Another form of cell death is necrosis, a passive and energy-independent process characterized by some morphological changes such as cell swelling, formation of cytoplasmic vacuoles, distended endoplasmic reticulum, condensed, swollen or ruptured mitochondria, disrupted organelle membranes, swollen and ruptured lysosomes and eventually disruption of the cell membrane (**Figure 10**). In humans, it has been reported that necrosis generally occurs in response to severe changes in physiological conditions, including hypoxia, ischaemia, hypoglycemia, nutrient deprivation, extreme temperature changes as well as exposure to ROS or toxins (Elmore 2007).

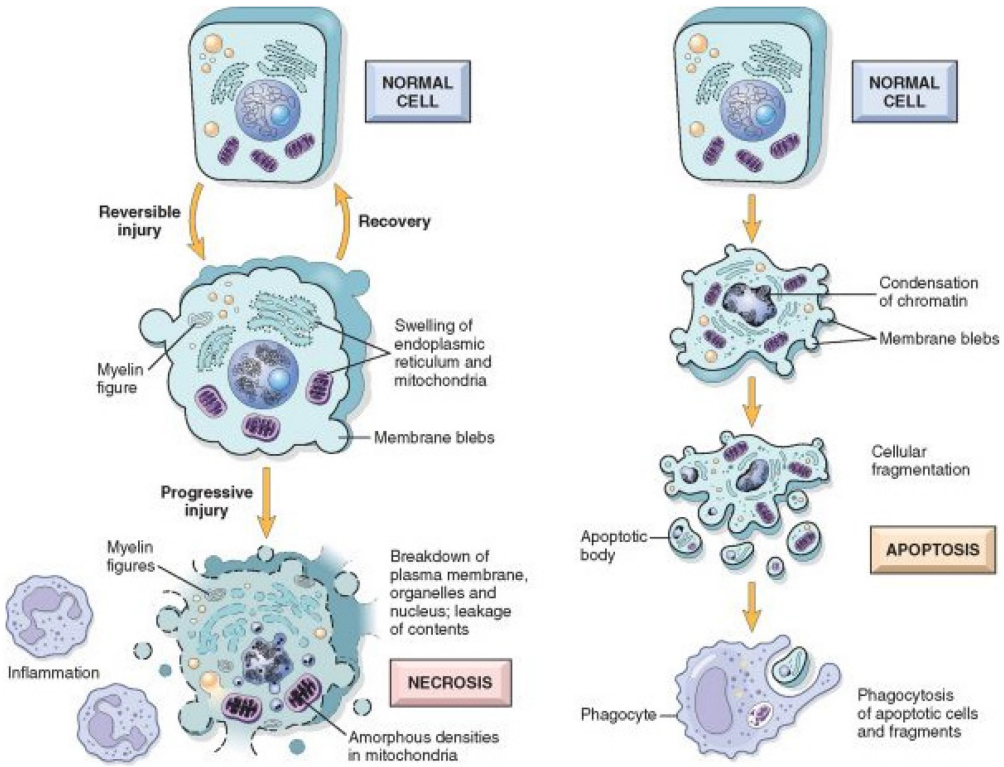

Figure 10. Comparison of morphological changes during apoptosis and necrosis.

Several authors have reported that hydroxytyrosol can induce later apoptosis and necrosis in different cancer cells such as colon cancer cells (Caco-2 and HT-29) and papillary and follicular thyroid cancer cells (López de las Hazas et al., 2017; Toteda et al., 2016).

In addition, other authors have reported that hydroxytyrosol induces an increase in cleaved PARP1, cleaved caspase-3 and cleaved caspase-7 expression in colorectal adenocarcinoma DLD1 cells (Sun et al., 2014).

Similar results have been reported by Zubair et al., 2017, who have also shown that hydroxytyrosol induces a down-regulation of expression of anti-apoptotic proteins, Bcl-2 and Bcl-xL, in a dose-dependent manner with simultaneous induction of Bax, thereby leading to an increase in the ratio of Bax/Bcl-2 as well as Bax/Bcl-xL in prostate cancer cells.

Toteda et al., 2016 have also reported the involvement of the mitochondrial apoptotic pathway due to a significant up-regulation of caspase-9, cyt c release from the mitochondria to cytosol and an up-regulation of p53 and BAD proteins expression.

1.3.4 Epigenetic modulation

It is well known that polyphenols are able to modulate the epigenetic status (Pan et al., 2013) even if very few data on epigenetic effects induced by hydroxytyrosol are present in literature (Cetrullo et al., 2016; D'Adamo et al., 2017; Yang et al., 2017; Wang et al., 2018; Zhi et al., 2018).

The epigenetics could be defined as the study of mechanisms which alter gene expression without altering the primary DNA sequence. Epigenetic mechanisms are heritable and reversible, and include changes in DNA methylation, in histone modifications and in the production of small non-coding microRNAs (miRNA). It has been demonstrated that aberrant epigenetic mechanisms may lead to several pathological conditions; in particular in cancer alterated methylome, both hypo- and hypermethylation have been observed (Kanwala and Gupta, 2012).

DNA methylation, which is essential for physiological processes, consists of the covalent addition of a methyl group from S-adenosyl-methionine (SAM) at the 5 position of the cytosine catalyzed by DNA methyltransferases (DNMTs) (**Figure 11 A**). Generally 5-methylcytosines are observed within CpG dinucleotides which are concentrated in large clusters called CpG islands, containing the promoter and/or the first exon region. Normally, the CpG islands are unmethylated in transcriptionally active genes, whereas they are methylated in silenced genes (Kulis and Esteller, 2010) (**Figure 11 B**).

In normal cells, pericentromeric heterochromatin is highly methylated; satellite sequences and repetitive genomic sequences are silenced, ensuring genomic integrity and stability. In different tumors the loss of DNA methylation of normally inactivated regions has been

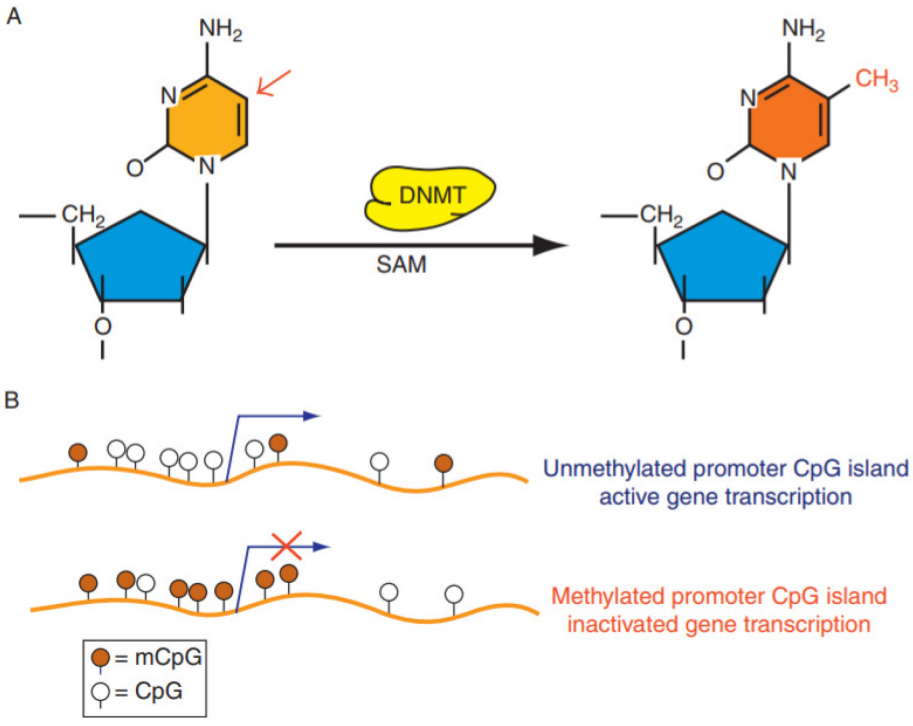

Figure 11. Cytosine methylation (Kulis and Esteller, 2010)

observed, leading to mutagenesis and genomic instability (Costa et al., 2006). However, certain genes undergo inactivation as a consequence of hypermethylation of CGIs in regulatory regions, which are unmethylated in normal cells. Various tumor-suppressor genes silenced by DNA hypermethylation have been identified in tumor tissues (Greger et al., 1989).

Histone modifications are post-translational covalent additions to the N-terminal and C-terminal of histone tails; however, some modifications can occur within the globular domain. Currently, different types of histone modifications - including acetylation, methylation, phosphorylation, ubiquitination, sumoylation, ADP ribosylation, deimination, proline isomerization and propionylation - have been identified (Kouzarides, 2007).

It has been reported that histone acetylation, first discovered by Allfrey et al. (1964), is an N^{ε}-acetylation of lysine, controlled by two enzymes - histone acetyltransferases (HATs) and histone deacetylases (HDACs). The lysine acetylation neutralizes the positive charge of histone tail, weakening histone–DNA or nucleosome–nucleosome interactions, thus facilitating the access to the DNA for different nuclear factors, such as the transcription complex. In contrast, the histone deacetylation decreases the accessibility for transcription factors between nucleosome and DNA (**Figure 12**). Changes in histone modifications have also been detected in different cancer types. (Sawan and Herceg, 2010). In examining epigenetic modification induced by hydroxytyrosol-enriched fraction from OMWW in our experimental model, we chose two approaches: 1) global methyloma analysis by Comet assay; 2) sirtuins expression/activity.

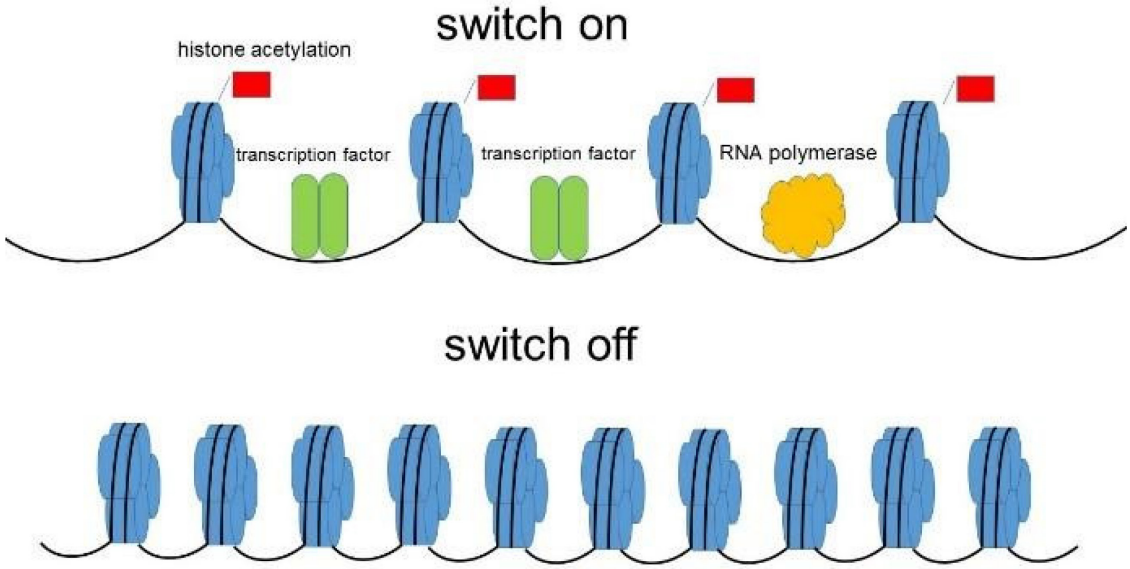

Figure 12. Histone acetylation and deacetylation

Mammalian sirtuins, NAD^+-dependent deacetylases and mono-[ADP-ribosyl] transferases, are a family of 7 members (SIRT1-7) differing in their localization, activity and functions. In particular, SIRT1, SIRT6 and SIRT7 are mainly nuclear; SIRT2 and SIRT3 are mainly cytoplasmic and mitochondrial, respectively, although they are present in the nucleus only at low levels; SIRT4 and SIRT5 are present in the mitochondria.

Mammalian sirtuins are involved in the chromatin regulation, cell survival under stress, metabolic homeostasis regulation, and developmental and cell differentiation (Vaquero and Reinberg, 2008). Under chronic stress, SIRT1, SIRT2 and SIRT3 can protect the organism by inducing cell senescence or apoptosis (**Figure 13**) (Bosch-Presegué and Vaquero, 2011). SIRT1, the most studied sirtuin, regulates both types of p53-mediated apoptosis (p53-transcriptional dependent and p53-transcriptional independent). Numerous studies have evidenced that sirtuins, especially SIRT1, have a dual role in cancer, operating as tumor suppressors or as an oncogenic factor.

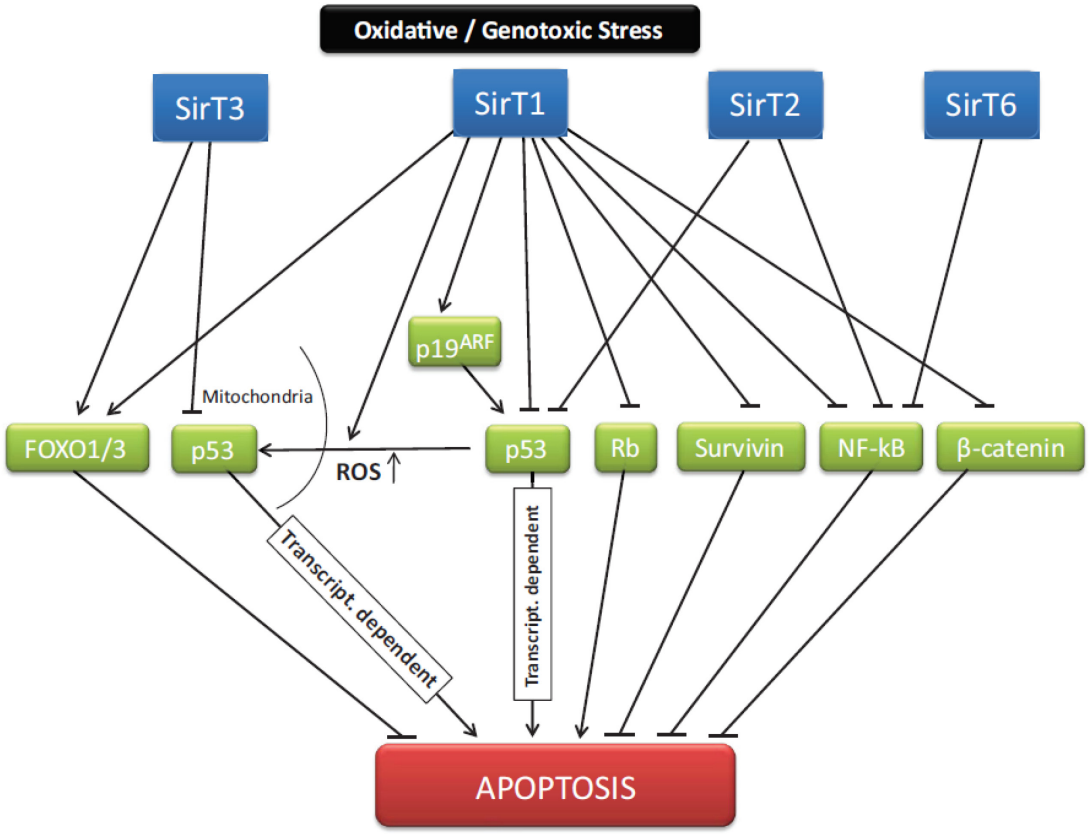

Figure 13. Sirtuins and cell survival (Bosch-Presegué and Vaquero, 2011)

1.4 Cell lines

1.4.1 MRC-5 cell line

MRC-5 is a human fibroblasts cell line derived from normal lung tissue of a 14-week-old male fetus by J.P. Jacobs in September of 1966 (**Figure 14**). This is a diploid cell line with normal X and Y chromosomes. The rate of polyploidy is 3.6%. MRC-5 cell line is sensitive to infection of a large variety of viruses and it is commonly used in the production of viral vaccines (Alirezaie et al., 2011; Jacobs JP. 1976; Mirchamsy et al., 1976). In addition, MRC-5 cells have already been used in cosmetic field to evaluate anti-UVA effect of different plant extracts as reported by patent US 2003/0072820 A1.

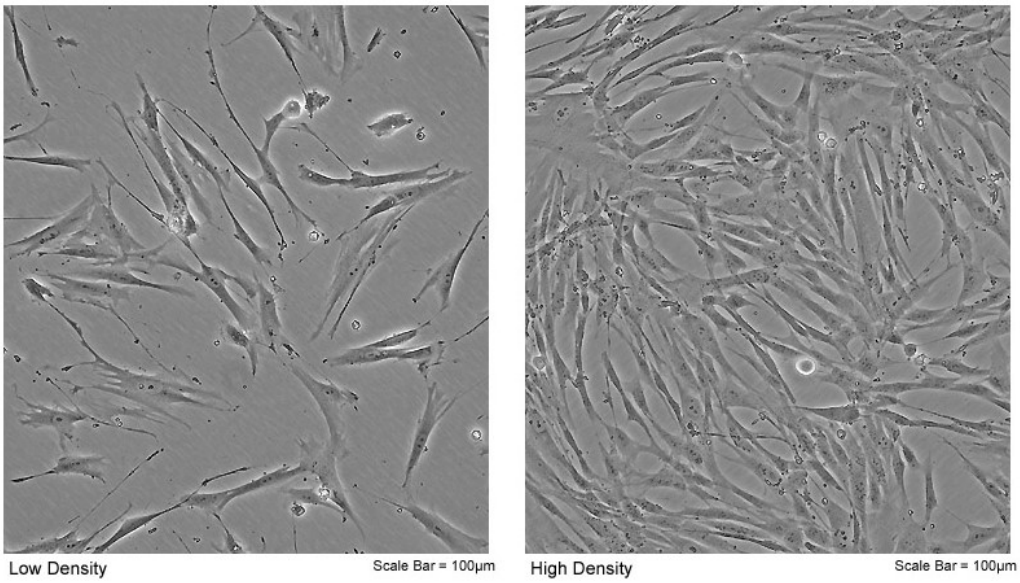

Figure 14. Images of MRC-5 cells.

1.4.2 1321N1 cell line

1321N1 is a human astrocytoma cell line (**Figure 15**) isolated in 1972 as a sub clone of the cell line 1181N1 which in turn was isolated from the parent line U-118 MG (one of a number of cell lines derived from malignant gliomas by J Ponten (Pontén and Macintyre, 1968).

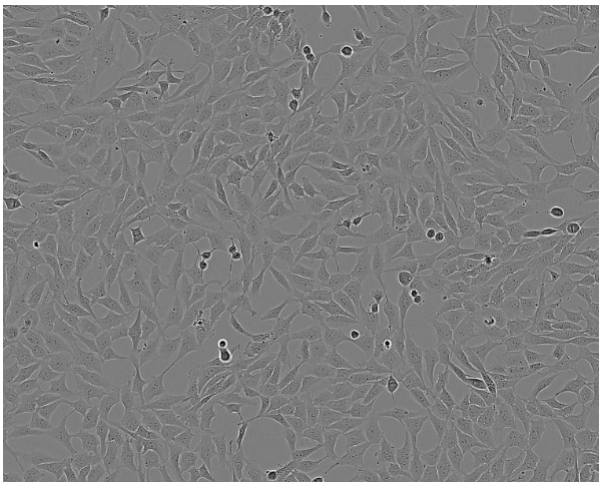

Figure 15. Image of 1321N1 cells.

1321N1 has been shown to have very similar STR profile data to U-118 MG. It is well known that astrocytoma is the leading CNS tumor in children. In particular, low-grade astrocytomas are responsible for approximately one third of cases and are classified as WHO grade I (well circumscribed with only a narrow margin of infiltration into the surrounding tissues) and WHO grade II (infiltrative). High-grade astrocytomas comprise approximately 7-11% of pediatric tumors and are classified as WHO grade III (e.g. anaplastic astrocytoma) and WHO grade IV (e.g. glioblastoma) (Isaacs, 2016).

CHAPTER II

AIMS

Due to the importance of olive oil in the economy of Sicily, our group together with the Institute of Biomolecular Chemistry (Italian National Research Council, Catania) have been trying to evaluate the potential use of some fractions obtained from OMWW in cosmeceutical and nutraceutical field.

Indeed, the aims of my doctorate project were to evaluate:

1) some possible differences between the chemical composition of two OMWW generated from Sicilian olive cultivar (Cerasuola and Nocellara etnea);

2) safety and the moisturizing properties of a sugars and minerals enriched fraction (SMEF), obtained from Cerasuola-OMWW, by *in vitro* and *in vivo* studies;

3) the chemotherapeutic activities *in vitro* exhibited by hydroxytyrosol-enriched fraction (H-EF) obtained from Cerasuola-OMWW. As control, we used hydroxytyrosol commercial standard (HTyr).

CHAPTER III

MATERIALS AND METHODS

3.1 Materials

Cerasuola-OMWW and Nocellara etnea-OMWW were freshly collected from three-phase olive oil mill processing systems located respectively in Menfi (Agrigento, Italy) and in Mascalucia (Catania, Italy). Folin-Ciocalteu reagent, 1-diphenyl-2-picrylhydrazyl (DPPH), 3-(4,5-dimethylthiazol-2-yl)-2,5-diphenyltetrazolium bromide (MTT), trifluoroacetic acid (TFA), activated charcoal and all standards were purchased from Sigma-Aldrich (St. Louis, MO, USA). HPLC grade solvents were purchased from Carlo Erba (Italy). Purosorb™PAD428 resin was purchased from Purolite. The TUNEL Apoptosis Detection Kit-DNA Fragmentation/Fluorescence Staining was purchased from Merck Millipore (Germany). The Nuclear Extraction Kit (ab113474) and the Universal SIRT Activity Assay Kit (ab156915) were purchased from Abcam. All other chemicals were purchased from Sigma-Aldrich (St. Louis, MO, USA) and Gibco-BRL Life Technologies (Grand Island, NY, USA).

3.2 Methods for chemical analysis of OMWW

3.2.1 OMWW pretreatment and physicochemical analysis

OMWW were centrifuged at 4000 rpm for 20 minutes and the supernatant was filtered through filter paper under vacuum condition. Filtered OMWW were stored at -20°C before use. The pH values of OMWW samples were determined by using a Mettler Toledo

SevenCompact pH meter. Chemical Oxygen Demand (COD), total nitrogen, total phosphorous and metals were determined according to EPA (U.S. Environmental Protection Agency) methods 410.3, 352.1, 365.3 and 200.8.

Total sugars were determined according to Dubois method (Dubois et al., 1956; Fava et al., 2017). The absorbance was measured at λ 490 nm and compared against a glucose calibration curve (R^2=0.999) (Cary UV Agilent Technology). Results were expressed as g/l of glucose.

3.2.2 Total phenolic content

The total phenolic content of OMWW samples was determined using the Folin-Ciocalteu assay (Folin, 1927; Marinova et al., 2005; Singleton and Rossi, 1965). Briefly, 10 µl of OMWW or gallic acid standard solution, appropriately diluted, were added to 90 µl of water. Folin-Ciocalteu reagent (10 µl) was added to the mixture and shaken. After 5 minutes, 100 µl of 7% (w/v) Na_2CO_3 were added and the obtained solution was diluted with water up to 250 µl, shaken and incubated for 90 minutes at room temperature. The absorbance was determined at λ 750 nm with a microplate spectrophotometer reader (Synergy HT multi-mode microplate reader, BioTek, Milano, Italy) and compared against a gallic acid calibration curve (y=0.002x+0.030, R^2=0.9997). The total phenolic content was expressed as g/l of gallic acid.

3.2.3 Total flavonoid content

An aliquot (25 µl) of OMWW or gallic acid standard solution, appropriately diluted, was transferred to test tube containing 100 µl of water. At time zero, 7.5 µl of 5% (w/v) $NaNO_2$ were added; at 5 minutes 7.5 µl of 10% (w/v) $AlCl_3$ were added; finally, at 6 minutes 50 µl of 1 M NaOH were added. Each reaction mixture was diluted with water up to 250 µl and

mixed (Salerno et al., 2014). The absorbance was measured at λ 510 nm with a microplate spectrophotometer reader (Synergy HT multi-mode microplate reader, BioTek, Milano, Italy) and compared against a catechin calibration curve (y= 0.0008x-0.0094, R^2 = 0,9968). The total flavonoid content was expressed as g/l of catechin.

3.2.4 HPLC-DAD analysis

The chromatographic analysis of polyphenolic compounds was performed by HPLC-DAD (HITACHI) using a Kinetex C-18 (4.6x250mm, 5µm) column (Phenomenex) with a security guard cartridge (Phenomenex), thermostated at 30°C±1°C. The samples were eluted with water (A) and acetonitrile (B) both added with 0.1% trifluoroacetic acid (TFA) according to the following gradient: 100% A as initial condition, maintained for 5 minutes; 58% A in 25 minutes; 100% B in 15 minutes, maintained for 5 minutes. The flow rate was 0.8ml/min. The chromatograms were acquired at 280nm. The polyphenolic compounds were identified by comparison of retention times and UV spectra with the corresponding commercial standards: gallic acid, hydroxytyrosol, tyrosol, 4-hydroxybenzoic acid, 4-hydroxyphenylacetic acid (PHPA), caffeic acid, vanillic acid, floretic acid, verbascoside, p-coumaric acid, trans-ferulic acid, oleuropein, catechol, 4-hydroxybenzoic acid, 4-methylcatechol, 3-hydroxyphenylpropionic acid, 3,4,5-trimethoxybenzoic acid and trans-cinnamic acid. A 5-points calibration curve of each standard was used for the quantification.

3.2.5 Antioxidant activity of OMWW

The antioxidant activity of OMWW was evaluated by DPPH assay (Blois 1958; Salerno et al., 2014). The reaction mixture contained DPPH radical (86 µM) and different amounts of OMWW in 1 ml of ethanol to obtain concentrations of OMWW, expressed as µM of hydroxytyrosol, ranging from 1 to 100 µM. The samples were incubated for 10 minutes at

room temperature, then the absorbance was measured at λ 517 nm with a microplate spectrophotometer reader (Synergy HT multi-mode microplate reader, BioTek, Milano, Italy). The results were expressed as percentage decrease in absorbance with respect to control. Hydroxytyrosol was used as standard.

3.2.6 Stability studies

The stability of OMWW samples stored in the dark at different temperatures (-20°C, 4°C and 25°C) under aerobic conditions was evaluated by measuring total phenols, total flavonoids and hydroxytyrosol content as previously described.

3.3 Methods for cosmeceutical application

3.3.1. Preparation of sugars and minerals enriched fraction (SMEF)

An aliquot of filtered Cerasuola-OMWW (500 ml) was passed through a column (80x4cm) filled with 200 g of Purosorb™PAD428 and eluted with water (700 ml) with a flow of 0.5ml/min. The aqueous fraction was lyophilized and the adsorbent was washed with ethanol, dried and stored at room temperature.

3.3.2 Chemical characterization of SMEF lyophilized fraction

Chromatographic analysis of sugars

The characterization of sugars present in the lyophilized fraction was performed by HPLC-ELSD (HITACHI, High-Technologies Corporation) as reported by Shanmugavelan et al. (2013), with slight modifications. The HPLC analysis was performed using a Prevail Carbohydrates ES (250x4.6mm, 5µm) column (Alltech) thermostated at 25°C±1°C. The sample was eluted isocratically with acetonitrile/water (75/25 v/v) with a flow rate of 1

ml/min. Injection volume was 10 µl. Drift tube temperature was 45°C, nitrogen pressure was set to 4.1 bar.

The sugars were identified by comparison of retention times with the corresponding commercial standards (fucose, arabinose, xylose, fructose, mannose, galactose, glucose, sucrose and maltose). A second-order polynomial calibration curve of each standard (50-750 mg/l) was used for the quantification.

Metals Determination

A multiwave 3000 microwave sample preparation system equipped with 8XF100 rotor (Anton Paar GmbH, Graz, Austria, Europa) for sample mineralization was used. A total of 200 mg of each sample (SMEF lyophilized fraction and cosmetic emulsion) was loaded into fluoroplastic vessels (XF100 TFM or PFA) along with a digestion mixture containing 3.5 ml of HNO_3 and 1.5 ml of H_2O_2 according to EPA 3052 guidance (with opportune modification) and placed in a ceramic supporting vessel.

The mineralization program heated the samples for 30 minutes at a power of 800 W and then cooled them for 15 minutes. After cooling, the contents of the vessels were diluted to 10 ml with ultrapure water and filtered through a Whatman quantitative filter paper, ash less, grade 40. Metal concentrations were determined with an ICP/MS Nexion 300X (Perkin Elmer Inc. Waltham, Massachusetts, U.S.A) using the kinetic energy discrimination mode (KED) for interference suppression. Each determination was performed three times.

The accuracy of the analytical procedure was confirmed by measuring a standard reference material, Nist 1566B oyster tissue, without observing an appreciable difference. Before analytical measurement, appropriate calibrations were made and a “blank” was established. All concentrations are calculated as mg/kg.

3.3.3 In vitro study

Cell cultures and treatments

MRC-5 cells - the human fetal lung fibroblast cells - were obtained from the American Type Culture Collection (Rockville, MD, USA) and cultured in 25 cm^2 flasks and/or in 6-12- or 96-multiwell microplate, according to type of assay to be performed, with Eagle's Minimum Essential Medium (EMEM) supplemented with 10% Fetal Bovine Serum and (50IU/ml) penicillin/ (50µg/ml) streptomycin, and incubated at 37°C in a humidified atmosphere with 5% CO_2. The treatments were performed at subconfluence and then the cells were detached by trypsin and washed in PBS 1X by centrifugation. The cells were treated with SMEF at different concentrations (% w/w) prepared by dissolving the SMEF lyophilized fraction in culture medium at the appropriate final concentrations for each biological assay.

MTT assay

The potential cytotoxic effect of the lyophilized fraction was evaluated by MTT assay, a colorimetric method which measures the reduction of MTT, a yellow tetrazolium salt, to a purple formazan by the mitochondrial dehydrogenase enzyme of living cells (Malfa et al., 2010).

MRC-5 cells ($1x10^4$ cells/well) were treated with different concentrations of lyophilized SMEF in culture medium (0.5%, 1%, 2%, 5%, 10% w/w) for 6 and 24 hours; then 200 µl of MTT (0.5 mg/ml) in culture medium were added to each well and incubated for 3 hours at 37°C in a humidified atmosphere with 5% CO_2. The optical density (OD) was measured with a microplate spectrophotometer reader (Synergy HT multi-mode microplate reader, BioTek, Milano, Italy) at λ 550 nm. The results were expressed as percentage of cell viability with respect to untreated control viable cells, which value was equal to 100%.

TUNEL assay

Apoptosis was evaluated by TUNEL assay, a method which identifies apoptotic cells *in situ* by using terminal deoxynucleotidyl transferase (TdT) to transfer biotin-dUTP to the free 3'-OH of cleaved DNA, according manufacturer's protocol.

The assay was performed on MRC -5 cells untreated and treated with different concentrations of SMEF lyophilized fraction in culture medium (1%, 2% and 5% w/w), both for 6 and 24 hours. For each sample ten fields, randomly selected, were analyzed using an epifluorescence microscope (Leica, Wetzlar, Germany) equipped with a camera. The apoptotic index was calculated as the number of apoptotic cells in each field.

Alkaline comet assay

The potential genetoxic effect of lyophilized fraction was evaluated by single-cell gel electrophoresis, commonly called Comet assay (**Figure 16**).

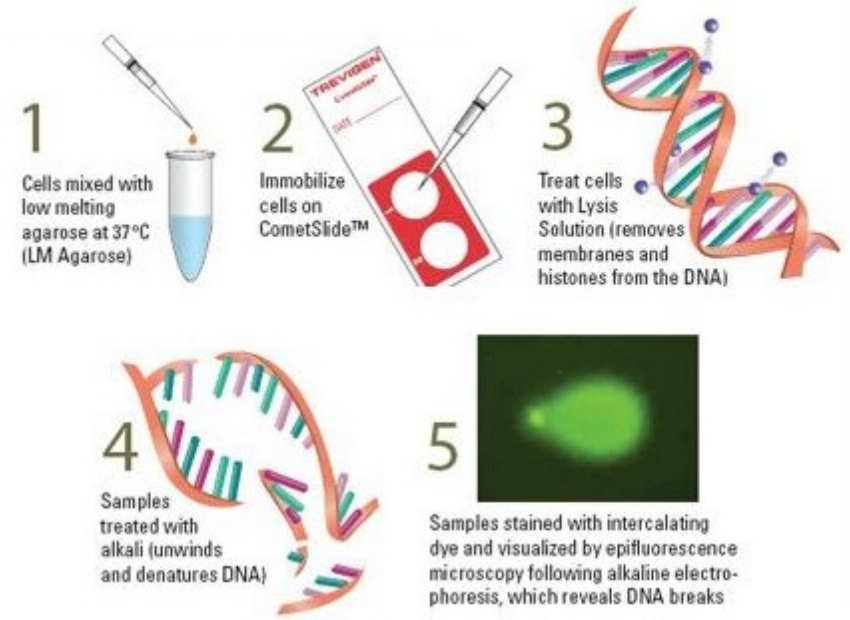

Figure 16. Comet assay

It is a simple and sensitive method for assessing DNA damage at the single-cell level. According to various versions, it is possible to evidence different types of damage. For instance, the neutral comet assay allows to identify double stranded breaks; the alkaline comet assay (pH >13) is capable of detecting DNA double-strand breaks, single-strand breaks, alkali-labile sites, DNA-DNA/DNA-protein cross-linking, and incomplete excision repair sites. The inclusion of digestion of lesion-specific DNA repair enzymes in the procedure allows the detection of various DNA base alterations (Pu et al., 2015).

Alkaline comet assay was performed on MRC-5 cells untreated and treated with SMEF lyophilized fraction dissolved in culture medium (0.5%, 1%, 2% and 5% w/w), both for 6 and 24 hours, according to Malfa et al. (2010), with slight modifications. Briefly, cells embedded with 0.7% low melting point agarose (LMA) were deposited onto microscope slides pre-coated with 1% melting point agarose (NMA). After lysis and unwinding treatments, the nucleoids were electrophoresed for 20 minutes at 0.7 V/cm, washed with neutralization buffer, dried with 70% ethanol and stained with SYBR Green (1:10000). Fifty nucleoids were analyzed for each sample using an epifluorescence microscope (Leica, Wetzlar, Germany) equipped with a camera. CASP (1.2.2) image analysis software was used to evaluate DNA damage. The results were expressed as the percentage of fragmented DNA present in the comet tail (%TDNA) (**Figure 17**).

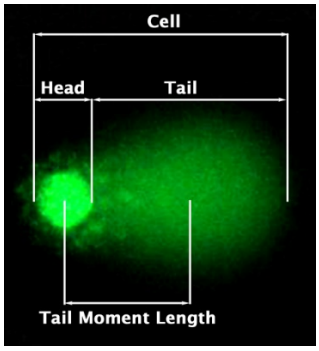

Figure 17. Nucleoid

Measurement of ROS

Intracellular ROS levels were evaluated by using of DCFH-DA, a non-fluorescent molecule able to spread through the cell membrane. Once inside the cell, esterases hydrolyze the acetyl groups generating the non-fluorescent 2',7'-dichlorofluorescin (DCFH). Intracellular ROS are able to oxidize DCFH into fluorescent dichlorofluorescein (DCF).

MRC-5 cells (5 x10^5 cells/well) were treated with different concentrations of lyophilized SMEF in culture medium (0.5%, 1%, 2% and 5% w/w), both for 6 and 24 hours. After collection, the cell suspension was treated with DCFH-DA 5 µM for 30 minutes at 37°C in the dark, washed with PBS 1X and then analyzed by Flow Cytometry (EPICS XL-MCL, Beckman Coulter, California–USA) equipped with a 488 nm Argon laser. Instrument settings were checked daily using Flow-Check™ Fluorospheres (Beckman Coulter) as recommended by manufacturer. For each sample, 5000 events were analyzed by Expo32™ software (Beckman Coulter) and listmode data were analyzed by Kaluza software (Beckman Coulter). The dichlorofluorescein (DCF) upon excitation at 488 nm emits green fluorescence, proportional to the ROS intracellular levels, between 500 and 550 nm (Rothe and Valet, 1990; Sarkar et al., 2005). The results were expressed as the percentage of green fluorescent cells.

Scanning Electron Microscopy (SEM) cell morphology analysis

Morphological treatment-induced (0.5%, 1%, 2% and 5% w/w for 6 hours) cell alterations were determined by SEM analysis as described by Malfa et al. (2014). The cells were washed with Sodium Cacodylate Buffer 0.1 M (pH 7.4), fixed in 2% glutaraldehyde in 0.1 M PBS (pH 7.2) for 1 hour at 4 °C, rinsed in buffer and post-fixed in 1% Osmium tetroxide (OsO_4) in Sodium Cacodylate Buffer 0.1 M pH 7.4 for 1 hour at 4˚C. Then, the cells were washed with 0.1 M Sodium Cacodylate twice for 10 minutes and dehydrated with increasing ethanol

concentrations (30%, 50%, 70%, 95%, 100%). The cells were critical point dried with CO_2 (Emitech K850) and coated with gold. Cell morphology was examined with a scanning electron microscope (Zeiss EVO LS 10).

3.3.4 Formulation, metals analysis and long-term stability study

The lyophilized SMEF (1% w/w) was formulated in an oil-in-water (O/W) emulsion whose composition (F1), compared with base composition (F0) is shown in **Table 1**.

Table 1. Compositions of O/W emulsions

Ingredients (% w/w)	**F0**	**F1**
Water	71	70
Capric caprylic trygliceride	5	5
Octyl palmitate	5	5
Glycerolum vegetalis	5	5
Cetearyl Alcohol	3	3
Steareth 21	3	3
Stereath 2	2	2
Prunus dulcis oil	2	2
Olea europaea oil	1	1
Olea europaea unsaponificable oil	1	1
Xanthan Gum	1	1
Lyophilized SMEF	-	1
Phenossyethanol	0.5	0.5
Na-Benzoate	0.2	0.2
K-Sorbate	0.2	0.2
Na-dehydroacetate	0.1	0.1

F1: emulsion containing lyophilized sugars and minerals enriched fraction (SMEF)
F0: base emulsion

Metals analysis was performed on 200 mg of F1 emulsion as described in Materials and Methods Section 2.2.2. Different aliquots F0 and F1 (10 g) were stored at 25°C±2°C with 60±5% R.H. for 12 months and at 40°C±2°C with 60±5% R.H. for 6 months at light. The pH, phase separation and appearance were evaluated, at 25°C, on fresh and stored samples as reported by Garbossa and Maia Campos, 2016.

3.3.5 In vivo evaluation of moisturizing properties

A panel of 30 healthy female volunteers (average age 28±5) were enrolled in accordance with the Declaration of Helsinki. After giving their informed consent, they were divided in two subgroups, A and B, each of 15 volunteers. Inclusion criteria were age and skin which had not been treated in the previous five weeks. Exclusion criteria were if participants presented skin disorders such as infections, dermatitis, psoriasis, and similar. The skin conditions were selected by clinical assessment criteria currently used in practice (Springett and Merriman, 1995). The volunteers were instructed both to apply the assigned emulsion (20 mg) on forearms twice a day and not to apply any topical products in the same area 24 hours before the beginning and throughout the test period.

We set a randomized, controlled, single-blind study where Group A applied F1 emulsion while group B applied F0 emulsion. Skin hydration was evaluated by MoistureMeterD Compact (Delfin Technologies Ltd, Finland) both before application and after 7 days. All measurements (four per area) were performed at 25°C±2°C with 35±5% R.H. The % increase of hydration for each group was calculated by this formula $[(V_{7d} - V_{0d})/V_{0d}) \times 100]$, where V_{0d} and V_{7d} are the average values of skin hydration at Day 0 and after 7days, respectively.

3.4 Methods for nutraceutical application

3.4.1 Preparation of hydroxytyrosol-enriched fraction (H-EF)

H-EF was obtained from Cerasuola-OMWW as described by Fava et al., 2017. Briefly an aliquot of filtered OMWW (50 ml) was passed through a column (25x2.5cm) filled with 10 g of activated charcoal. The sample was eluted with water to collect the unabsorbed fraction and then with ethanol (200 ml) to collect H-EF. The ethanolic fraction was dried under vacuum using a rotary evaporator and dissolved in water (50 ml). Finally, the adsorbent was regenerated with NaOH 1M, washed with water, dried and stored at room temperature.

3.4.2 In vitro study

Cell cultures

1321N1 cells, the human astrocytoma cells, were cultured with MEM supplemented with 10% Fetal Bovine Serum, 2% glutamine and (50IU/ml) penicillin/ (50µg/ml) streptomycin. The cells were cultured in 25 cm^2 flasks and/or in 6- or 96-multiwell microplate, according to type of assay to be performed and incubated at 37°C in a humidified atmosphere with 5% CO_2.. The treatments with H-EF (50, 100 and 200 µM) or hydroxytyrosol commercial standard (HTyr 100 µM) for 24 and 48 hours were performed at subconfluence and then the cells were detached by trypsin and washed in PBS 1X by centrifugation.

MTT assay

The cytotoxic effect of H-EF or Htyr was evaluated by MTT assay on 1321N1 (Malfa et al., 2010). The cells ($1x10^4$ cells/well) were treated with different concentrations of H-EF (50, 100 and 200 µM) or HTyr (100 µM) for 24 and 48 hours; then the assay was performed as already described in the Section 2.3.3.

Wound Healing assay

The effect of H-EF on 1321N1 migration was determined *in vitro* by Wound Healing assay. Confluent monolayers of 1321N1 cells in 12-well plates were wounded with a pipette tip and washed with PBS 1X to remove detached cells. The wounded monolayers were treated with H-EF (50 and 100 μM) or HTyr (100 μM) for 24, 48 and 72 hours. On the external surface of the plate's bottom, the wound area was marked with a dot as reference. The area next to the dot was photographed by a phase-contrast microscope at 24, 48 and 72 hours after wounding. Wound closure was quantified by measuring the remaining denuded area with the ImageJ software program (Version 1.43; Broken Symmetry Software, Bethesda, MD).

Cell cycle analysis

Cell cycle analysis was performed on untreated and treated cells as reported by Malfa et al., 2010. After the treatments, the cells were fixed in 75% ethanol and kept at -20°C for at least 2 hours. washed twice with PBS 1X and incubated in propidium iodide solution at 37°C for 20 minutes in the dark prior to flow cytometry analysis (EPICS XL-MCL, Beckman Coulter, California–USA), using the propidium iodide channel. Instrument settings were checked daily using Flow-Check™ Fluorospheres (Beckman Coulter) as recommended by manufacturer.

Lactic dehydrogenase release

Lactic dehydrogenase (LDH) release was measured spectrophotometrically in the culture medium and in the cellular lysates at λ 340 nm by analizing NADH reduction (Acquaviva et al., 2016). The percentage of LDH release was calculated as the percentage of the total

amount, considered as the sum of the enzymatic activity present in the cellular lysates and that in the culture medium.

Alkaline comet assay

Alkaline comet assay was performed on untreated and treated cells as described by Malfa et al. (2010) and already described in Section 2.3.3.

ROS determination

ROS levels were evaluated on untreated and treated cells using 2',7'-dichlorofluorescein diacetate (Acquaviva et al., 2016). 132N1 cells were seeded in 6-well plates (about 400000 cells per well) and incubated at 37°C in a humidified atmosphere with 5% CO_2.. After 24 hours, the cells were then treated with different concentrations of H-EF (50 and 100 μM) or Htyr 100 μM for 24 and 48 hours. Subsequently, the culture medium containing the treatments was removed and, after washing with PBS 1X, 500 μl of culture medium containing DCFH-DA at the final concentration of 5 μM are added to each well. After incubation at 37°C in a humidified atmosphere with 5% CO_2 for 20 minutes, the medium is transferred to a tube and centrifuged at 1350 rpm for 10 minutes; after centrifugation, the supernatant is removed and the pellet is resuspended with 500 μl of a digitonin solution (2.5 mg / mL). Then 500 μl of the digitonin solution (2.5 mg / mL) were added to each well and the content of each tube is combined with that of the respective well. After incubation for 1 hour in the dark at 4 ° C, the cells were scraped and the contents of each well were transferred to an eppendorf; subsequently the samples were centrifuged at 14000 rpm at 4 ° C for 10 minutes to eliminate the cellular residues which could interfere with the spectrofluorimetric reading. Finally, 200 μL of supernatant for each sample (or white digitonin solution) were transferred to a 96-well black plate to proceed with the spectrofluorimetric reading λ-

excitation = 488 nm, λ emission = 525 nm (Synergy HT multi-mode microplate reader, BioTek, Milan, Italy). The total protein content was evaluated for each sample according to Bradford (1976). The results were expressed as fluorescence intensity (FI) per mg proteins and compared with the untreated control cells.

Thiol groups determination

Thiol groups, containing predominantly reduced glutathione (GSH), were determined spectrophotometrically at λ 412 nm using 5,5′-dithiobis(2-nitrobenzoic acid) (Acquaviva et al., 2016). 132N1 cells were seeded in 6-well plates (about 400000 cells per well) and incubated at 37°C in a humidified atmosphere with 5% CO_2.. After 24 hours, the cells were then treated with different concentrations of H-EF (50 and 100 μM) or Htyr 100 μM for 24 and 48 hours. After the treatments, the cells were detached by trypsin and centrifuged at 500 g for 5 minutes. The pellet was washed with PBS 1X, centrifuged at 500 g for 5 minutes and resuspended in 100 μL of buffer (Tris base 0.25 M, EDTA 20 Mm, pH 8.2). The cells were sonicated 3 times for 10 seconds at the minimun output. DTNB solution 10 mM was prepared in ethanol and diluted 1:80. Then 320 μL of DTNB solution, 60 μL of buffer and 20 μL of lysate were mixed and incubated for 20 minutes at room temperature in the dark. The blank was prepared by adding 80 μL of buffer to 320 μL of DTNB solution. Subsequently, the samples were centrifuged at 3000 g for 10 minutes at room temperature. Finally, 200 μL of supernatant from each sample was transferred to a 96-well plate to measure the absorbance at 412 nm.

The total protein content present in the lysates was evaluated for each sample according to Bradford (1976). The results were expressed as nmol GSH/mg proteins calculated referring to a glutathione calibration curve.

Western Blot analysis

Whole cell protein extracts were prepared according to Laemmli (1970). The primary antibodies used were: anti-GAPDH (1:50000) (Millipore, Darmstadt, Germany), anti-p53 (1:500) (Santa Cruz Biotechnology, Santa Cruz, USA), anti-p21 (1:500) (Sigma-Aldrich, St. Louis, USA), anti-sirt 1 (1:250) (Cell Signaling Technology, Denvers, USA). The proteins target by primary antibodies were detected by using secondary horseradish peroxidase-conjugated antibodies (Dako, Glostrup, Denmark), diluted 1:2000, and an ECL system (Thermo Scientific, Rockford, USA). The level of individual proteins expression was measured by densitometric analysis using the software Image J and GAPDH of each lane as reference value.

Determination of nuclear sirtuins activity

Nuclear sirtuins activity was evaluated by using Universal SIRT Activity Assay Kit (ab156915, Abcam). The absorbance was measured with a microplate spectrophotometer reader (Synergy HT multi-mode microplate reader, BioTek, Milano, Italy) at λ 450 nm.

The activity for each sample was calculated according to the following formula:

$$[SIRT\ Activity\ (OD/min/mg)] = \left(\frac{Sample\ OD - NNC\ OD}{Protein\ Amount\ (\mu g)\ ^{*} \times min\ ^{**}}\right) \times 1000$$

* protein amount added in the reaction without inhibitor
** incubation time (90 minutes)

Nuclear extracts were obtained from untreated and treated cells by using ab113474 kit (Abcam).

Methy-sens Comet assay

Global DNA methylation was evaluated on untreated and treated cells by Methy-sens Comet. Two isoschizomeric restriction enzymes HpaII and MspI recognize the same tetranucleotide sequence (5'-CCGG-3') but display differential sensitivity to DNA methylation:

- HpaII is inactive when any of the two cytosines is methylated, but it is able to digest the hemimethylated 5'-CCGG-3' at a lower rate compared with the unmethylated sequences;
- MspI is able to digest 5'-C^{m}CGG-30 but not 5'- ^{m}CCGG-3' (Wentzel et al., 2010).

After lysis overnight at 4°C in the dark, the samples were incubated with 100 µl of Fast Digest HpaII e MspI (5µl/ml) (Fermentas) for 10 minutes at 37°C. Then the assay was performed as described in the Section 3.3.3. The global methylation was measured according the following formula:

$$\left(\frac{\%\text{TDNA HpaII}}{\%\text{TDNA MspI}} \right) \text{X } 100$$

3.5 Statistical Analysis

All the results were obtained by three independent experiments each performed in triplicate and the means and standard deviations for each value were calculated. Statistical differences among different treatments were assessed by One way Anova. Post hoc comparison was performed according to Bonferroni test. We applied $p<0.05$ as the minimum level of significance. All the analyses were performed using Graph Prism version 5.

Furthermore, Pearson test was applied to analyze the correlations between ROS level and each other parameters evaluated for the cosmeceutical application.

CHAPTER IV

RESULTS

4.1 Chemical analysis of OMWW

In **Table 2** are reported the data related to physicochemical characterization of Cerasuola-OMWW and Nocellara etnea-OMWW. Both OMWWs had a mildly acidic pH, 4.98-5.24 respectively, and high levels of COD, sugars, nitrogen and phosphorous.

Metals analysis performed by ICP-MS showed that potassium was the most abundant element in both waters.

Table 2. Physicochemical characterization of OMWW

	Unit	Cerasuola-OMWW	Nocellara etnea-OMWW
pH	-	4.98	5.24
COD	g/l	73.60	50.00
Total sugars	g/l	34.00	16.04
Total nitrogen	mg/l	350.00	116.00
Total phosphorous	mg/l	186.00	229.00
Metal:	mg/l		
▪ **Sb, Hg, As, Ag, Cd, Se, Bi, Be**		< 0.01	< 0.01
▪ **Mo**		0.01	0.02
▪ **Pb**		0.03	< 0.01
▪ **Al**		0.30	0.30
▪ **Cr**		0.02	0.01
▪ **Co**		0.02	0.01
▪ **Cu**		0.60	0.37
▪ **Zn**		3.00	2.28
▪ **Fe**		1.99	3.98
▪ **Mn**		2.17	1.24
▪ **Ni**		0.11	0.05
▪ **Na**		303.34	109.97
▪ **K**		7379.34	4732.58
▪ **Ca**		61.74	42.58
▪ **Mg**		240.56	161.41

The total phenolic and flavonoid contents of Cerasuola-OMWW and Nocellara etnea-OMWW are shown in **Table 3**. It is worth noting that Cerasuola-OMWW had a total phenolic and flavonoid content almost double compared to Nocellara etnea-OMWW. However, HPLC analysis evidenced that hydroxytyrosol and tyrosol were the most abundant biophenols present in both OMWW.

Table 3. Total phenolic and flavonoid content of OMWW

	Unit	Cerasuola-OMWW	Nocellara etnea-OMWW
Total phenolic content	g/l gallic acid	5.20±0.21	3.02±0.18
Total flavonoid content	g/l catechin	2.28±0.23	0.95±0.17
Gallic acid	mg/l	not identified	not identified
Hydroxytyrosol	mg/l	821.86	267.17
Pyrocatechol	mg/l	6.59	traces
Tyrosol	mg/l	105.93	37.49
***p*-Hydroxybenzoic acid**	mg/l	not identified	not identified
4-Hydroxyphenylacetic acid (PHPA)	mg/l	traces	traces
Caffeic acid	mg/l	9.12	10.42
Floretic acid	mg/l	21.17	33.87
Verbascoside	mg/l	traces	not identified
***p*-Coumaric acid**	mg/l	4.27	14.44
***trans*-Ferulic acid**	mg/l	not identified	2.35
Oleuropein	mg/l	14.32	Traces

The chromatograms, shown in **Figure 18**, highlighted a quantitative rather than a qualitative difference in the polyphenolic profiles of Cerasuola-OMWW and Nocellara etnea-OMWW. Moreover, a continuous low intensity band spreading along the chromatograms suggests the presence of a polyphenolic polymer as the origin of the OMWW dark pigmentation.

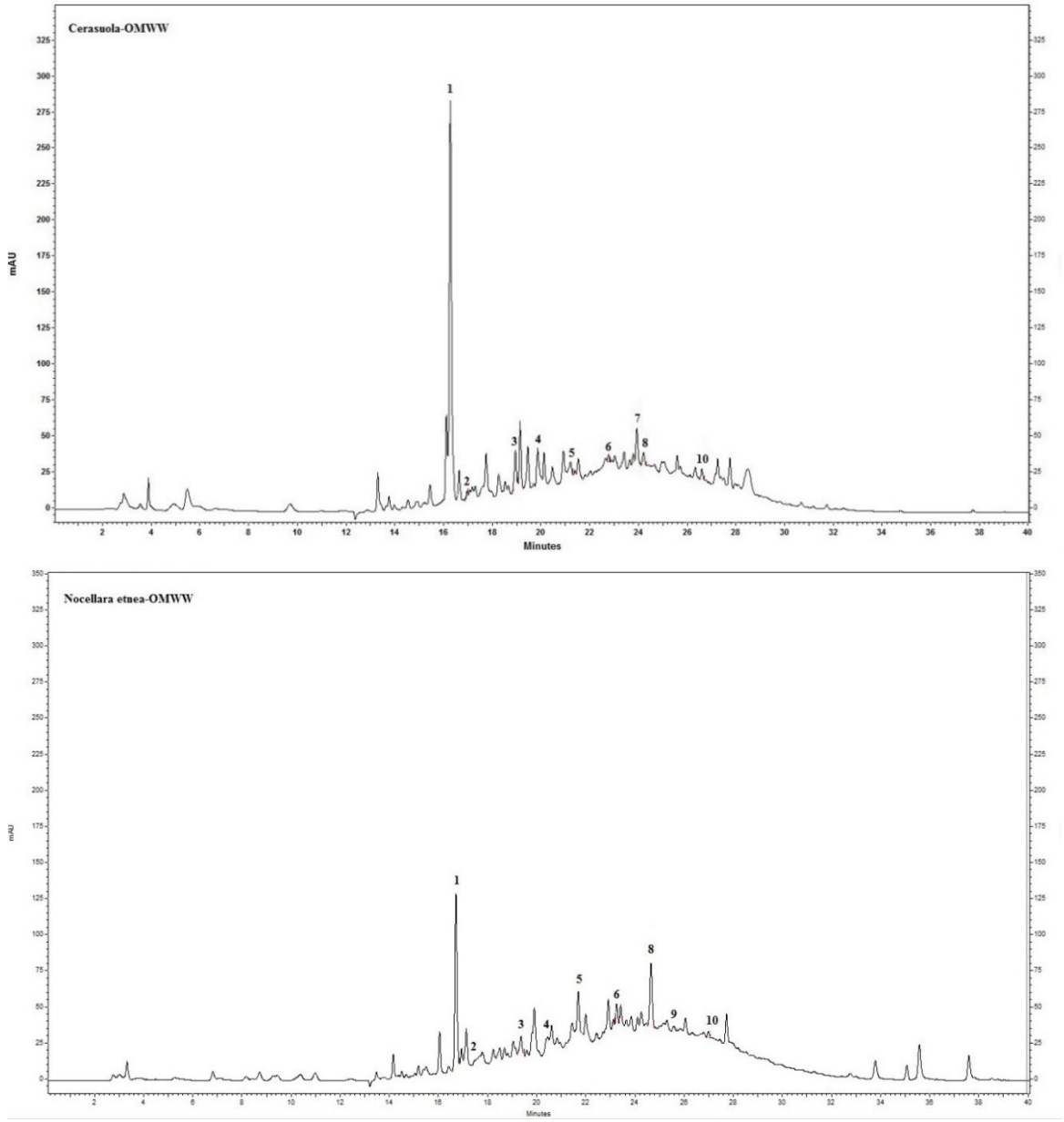

Figure 18. Chromatograms at 280 nm of Cerasuola-OMWW and Nocellara etnea-OMWW:
1) Hydroxytyrosol, 2) Pyrocatechol, 3) Tyrosol, 4) 4-Hydroxyphenylacetic acid (PHPA), 5) Caffeic acid, 6) Floretic acid, 7) Verbascoside, 8) *p*-Coumaric acid, 9) *trans*-Ferulic acid, 10) Oleuropein.

Figure 19 shows the antioxidant capabilities of Cerasuola-OMWW and Nocellara etnea-OMWW which were measured by DPPH test. The results, expressed as percentage decrease in absorbance with respect to control, evidenced the ability of the two waters in quenching, in a dose-dependent manner, the DPPH radical. In addition, both OMWW had a radical scavenging activity higher than the positive standard hydroxytyrosol ($p < 0.05$), probably

due to the synergistic effect of the other phenolic compounds present in the waters. Moreover, Cerasuola-OMWW showed a higher antioxidant activity with an IC_{50} value of 7.1 µM in comparison with Nocellara etnea-OMWW, as well as standard hydroxytyrosol, whose IC_{50} values were equal to 7.7 µM and 34.9 µM respectively.

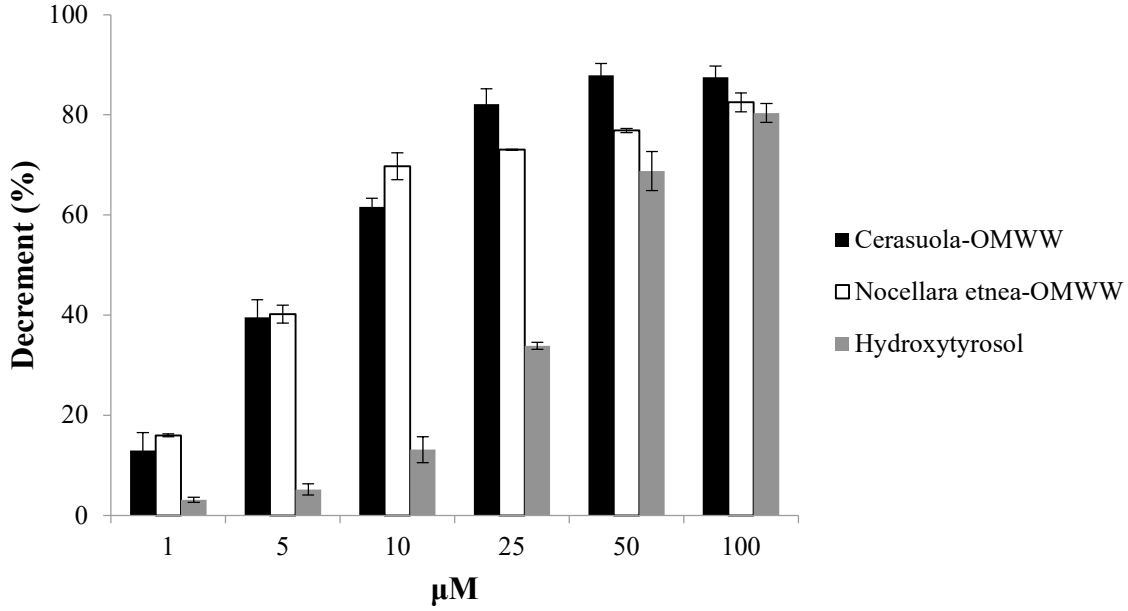

Figure 19. Antioxidant activity of Cerasuola-OMWW and Nocellara etnea-OMWW compared to hydroxytyrosol. The results, expressed as µM of hydroxytyrosol, are mean ± SD of three experiments each performed in triplicate. Both Cerasuola-OMWW and Nocellara etnea-OMWW values in the range 1-50 µM are significantly different ($p < 0.05$) *vs* hydroxytyrosol.

Table 4 reports the relative changes in the concentration of total phenols and flavonoids measured in Cerasuola-OMWW and Nocellara etnea-OMWW during their 45-day storage at different temperatures: 4°C and 25°C. The results evidenced a decrease of total phenols and total flavonoids, particularly in Nocellara etnea-OMWW, in a temperature- and time-dependent manner. No significant changes were observed with respect to total phenolic, flavonoid and hydroxytyrosol content in both OMWW samples stored at -20°C for 6 months (data not shown).

Table 4. Relative changes in the concentration of total phenols and flavonoids determined in Cerasuola-OMWW and Nocellara etnea-OMWW during storage at 4°C and 25°C.

	Days			
	0	**10**	**25**	**45**
Total phenols				
Cerasuola-OMWW (4°C)	100%	92.69%±0.79%[a]	79.16%±4.28%	76.84%±1.58%
Cerasuola-OMWW (25°C)	100%	81.09%±0.55%[a]	72.66%±3.15%	71.28%±5.96%
Nocellara etnea-OMWW (4°C)	100%	78.00%±1.17%[b]	68.85%±3.99%	67.44%±1.04%[b]
Nocellara etnea-OMWW (25°C)	100%	72.48%±1.44%[b]	65.65%±1.97%	64.52%±1.25%[b]
Total flavonoids				
Cerasuola-OMWW (4°C)	100%	81.57%±1.52%	78.36%±0.54%[c]	46.45%±3.30%
Cerasuola-OMWW (25°C)	100%	75.22%±2.33%	53.42%±1.78%[c]	41.59%±5.12%
Nocellara etnea-OMWW (4°C)	100%	59.30%±1.47%	56.34%±0.90%	56.34%±1.79%
Nocellara etnea-OMWW (25°C)	100%	58.88%±2.73%	58.88%±0.90%	57.61%±0.75%

The results are mean ± SD of three experiments each performed in triplicate. Values with a common letter within a column are significantly different ($p < 0.05$).

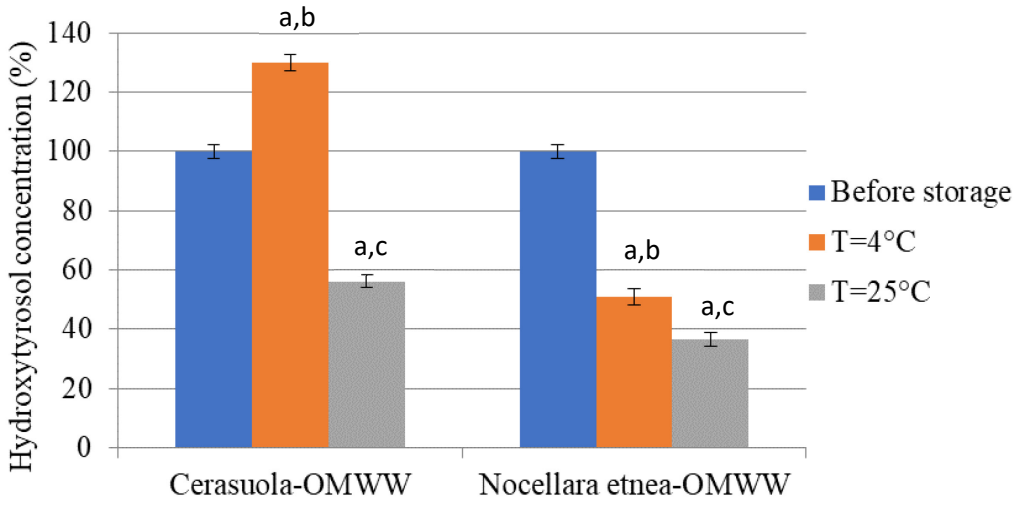

Figure 20. Relative changes in the hydroxytyrosol concentration determined in Cerasuola-OMWW and Nocellara etnea-OMWW after storage at 4°C and 25°C for 45 days. The results are mean ± SD of three experiments each performed in triplicate. Values with letter "a" are significantly different ($p < 0.05$) *vs* hydroxytyrosol concentration before storage; values with other common letters ("b" or "c") are significantly different ($p < 0.05$).

In addition, as reported in **Figure 20,** the measurement of the relative changes in the hydroxytyrosol concentration for both waters after their 45 days storage at 4°C and/or 25°C, evaluated by HPLC-DAD, evidenced: a) a decrease in hydroxytyrosol concentration in Nocellara etnea-OMWW samples stored at 4°C and 25°C; b) a slight increase in Cerasuola-OMWW samples stored at 4°C, probably due to the hydrolysis of oleuropein and verbascoside.

4.2 Studies for cosmeceutical application of lyophilized SMEF

Sugars composition and metal content have been examined in lyophilized fraction respectively by HPLC-ELSD and by ICP-MS.

Table 5. Sugars composition of lyophilized fraction evaluated by HPLC-ELSD

Monosaccharide	mg/100mg	Calibration curve
Fructose	2.8 ± 0.2	**y** = 36.267 x^2 +4917.269x –350090.333; $\mathbf{R^2}$=1.000
Mannose	8.2 ± 0.4	**y** = 22.001 x^2 +4856.762x –41040.577; $\mathbf{R^2}$=1.000
Glucose	31.8 ± 1.2	**y** = 13.441 x^2 +10298x –553244; $\mathbf{R^2}$=0.999

The values are mean ± SD of three experiments each performed in triplicate

Data obtained for sugar composition, as reported in **Table 5,** evidenced that glucose was the most abundant monosaccharide occurring in the fraction, followed by mannose and fructose. Metals content data, as reported in **Table 6,** evidenced potassium as the principal element, followed by sodium, magnesium and calcium.

The contents of Hg, Tl, Be, As, Ag, Cd, Bi and V were below 0.05 mg/kg; other metals were present in very small concentrations.

Table 6. Metals analysis of lyophilized fraction performed by ICP-MS.

Metal	mg/kg
Hg, Tl, Be, As, Ag, Cd, Bi, V	< 0.05
Mo	0.14 ± 0.01
Sb	0.08 ± 0.01
Pb	49.30 ± 0.96
Al	12.69 ± 2.71
Cr	1.99 ± 0.05
Co	0.33 ± 0.01
Cu	8.06 ± 0.04
Zn	54.95 ± 0.18
Sn	0.29 ± 0.02
Fe	54.41 ± 2.24
Mn	33.24 ± 1.78
Ni	2.16 ± 0.01
K	108767.7 ± 2800.2
Na	4552.4 ± 205.4
Mg	3542.3 ± 150.3
Ca	843.8 ± 25.2

The values are mean ± SD of three experiments each performed in triplicate

Figure 21 reports the MTT assay data obtained on human fibroblasts (MRC-5 cells) treated for 6 and 24 hours different concentrations of the lyophilized SMEF (0.5%, 1%, 2%, 5% and 10% w/w). As shown in the histograms, the lowest concentrations (0.5% and 1% w/w) did not influence cell viability either after 6 or 24 hours of treatment. Conversely, the highest concentrations (2%, 5% and 10% w/w) determined a drastic decrease of cell viability in a dose- and time-dependent manner.

The inspection of these results leads us to exclude, for the subsequent experimental phase, the use of the highest concentration (10% w/w), considered to be toxic.

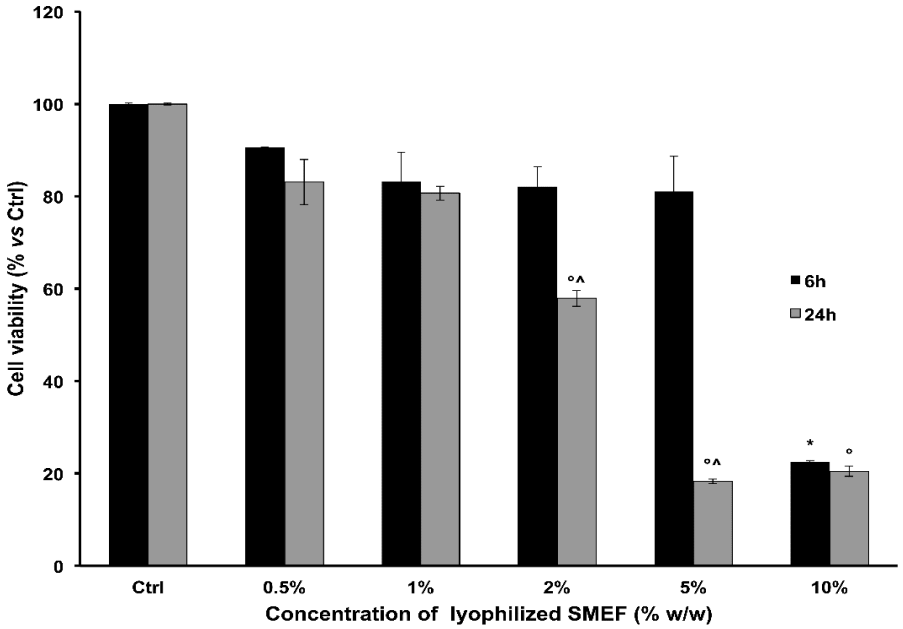

Figure 21. MTT assay performed on MRC-5 cells untreated and treated with different concentrations of the lyophilized SMEF (0.5%, 1%, 2%, 5% and 10% w/w) for 6 and 24 hours. The results, expressed as the percentage of cell viability with respect to untreated control cells (Ctrl), are mean ± SD of three experiments each performed in triplicate. *p < 0.05 vs. control group at 6 h; °p < 0.05 vs. control group at 24 h; ^p < 0.05 vs. same treatment at 6 h.

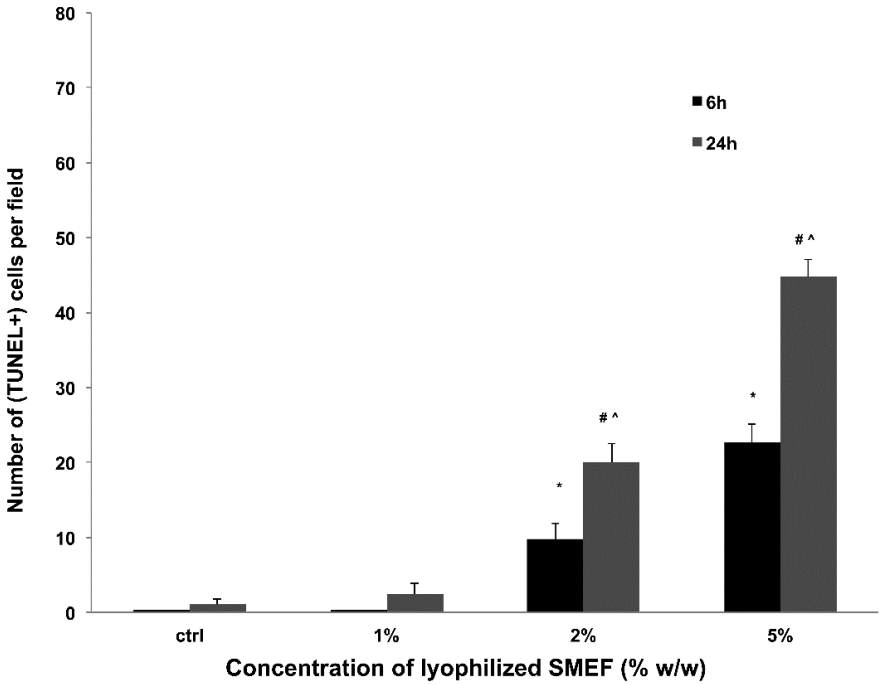

Figure 22. Quantitative analysis of (TUNEL+) MRC-5 cells treated with different concentrations of the lyophilized SMEF (1%, 2% and 5% w/w) at 6 h and 24 h. Reported data are means ± SD, n = 10 for each group. *p < 0.05 vs. control group at 6 h; #p < 0.05 vs. control group at 24 h; ^p < 0.05 vs. same treatment at 6 h.

The DNA damage extent was evaluated by alkaline Comet assay. As reported in **Figure 23**, DNA damage increased in a concentration-dependent manner (2% and 5% SMEF) without showing any change with respect to the treatment time.

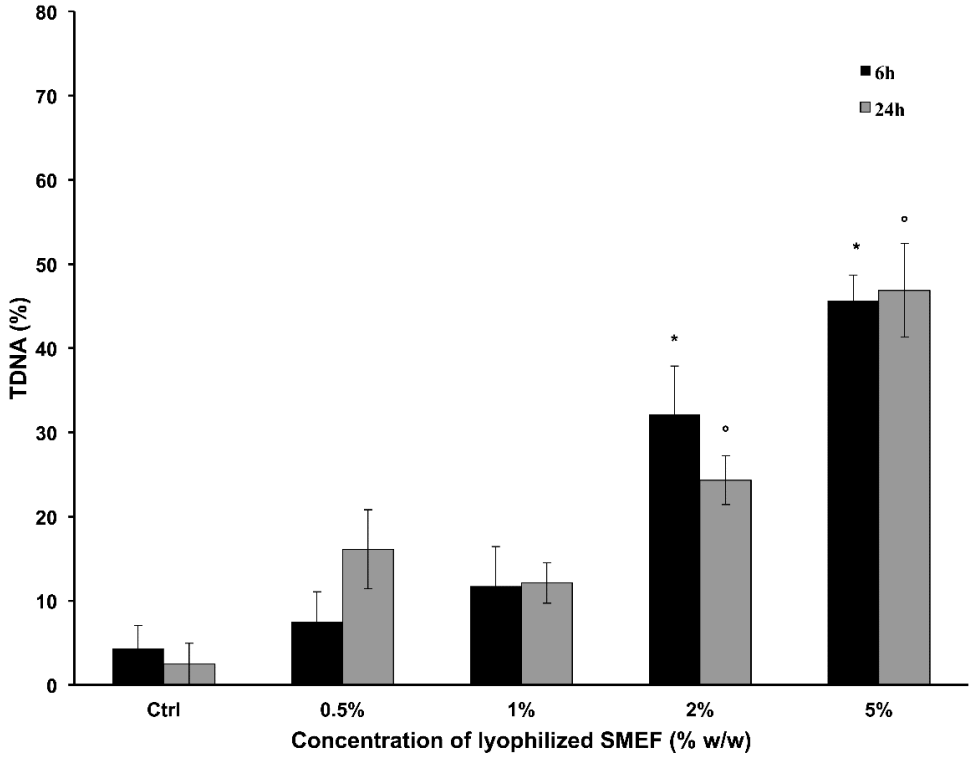

Figure 23. DNA damage evaluated by alkaline comet assay performed on both untreated and treated MRC-5 cells with different concentrations of the lyophilized SMEF (0.5%, 1%, 2% and 5% w/w) for 6 and 24 hours. The results are expressed as the percentage of DNA present in the comet tail (%TDNA). Values are mean ± SD of three experiments each performed in triplicate. *$p < 0.05$ vs. control group at 6 h; °$p < 0.05$ vs. control group at 24 h.

In order to elucidate the possible involvement of oxidative stress in the observed metabolic modulations induced by lyophilized SMEF, we investigated ROS production by flow-cytometric analysis. The results, reported in **Figure 24**, showed a significant increase in ROS production with respect to untreated control cells, in the presence of high concentrations of lyophilized SMEF (2% and 5% w/w).

In addition, Pearson test has evidenced a positive correlation between ROS levels with cell viability (r = 0.9661, p = 0.007), TUNEL+ cells (r = 0.9945, p = 0.005) and DNA fragmentation (r = 0.9540, p = 0.012) only at 24 hours.

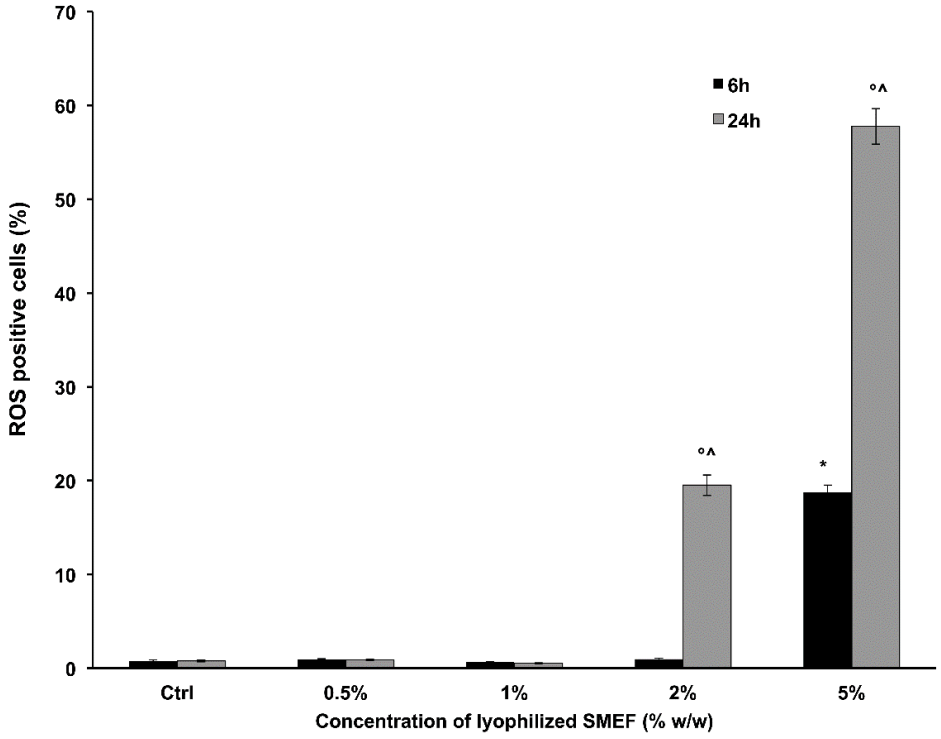

Figure 24. Percentage of ROS-positive cells after the treatment with different concentrations of the lyophilized SMEF (0.5%, 1%, 2% and 5% w/w) for 6 and 24 hours. Values are mean ± SD of three experiments each performed in triplicate. *p < 0.05 vs. control group at 6 h; °p < 0.05 vs. control group at 24 h; ^ p < 0.05 vs. same treatment at 6 h.

SEM analysis was performed only in fibroblasts treated for 6 hours in order to verify the presence of possible treatment-induced structural changes before biochemical response. In **Figure 25** the observed early alterations of cell morphology are shown.

A fusiform and fattened stellate morphology (**Fig. 25A**) with a large cytoplasm and a relatively smooth surface, except for few blebs or ruffles (**Fig. 25B**), is present in untreated fibroblasts. Moreover, they showed good adherence to the substrate by long filopodia. No significant difference was observed in cells treated with 0.5% and 1% w/w of lyophilized

SMEF compared to the control samples (data not shown). Fibroblasts treated with 2% and 5% w/w of lyophilized SMEF present remarkable morphological alterations proportionally to concentration increase. In particular, the cells tended to agglomerate leaving wide cell-free zones and showed an evident shrunken cytoplasm (**Fig. 25C, E**) with numerous blebs and ruffles on their surface (**Fig. 25D, F**).

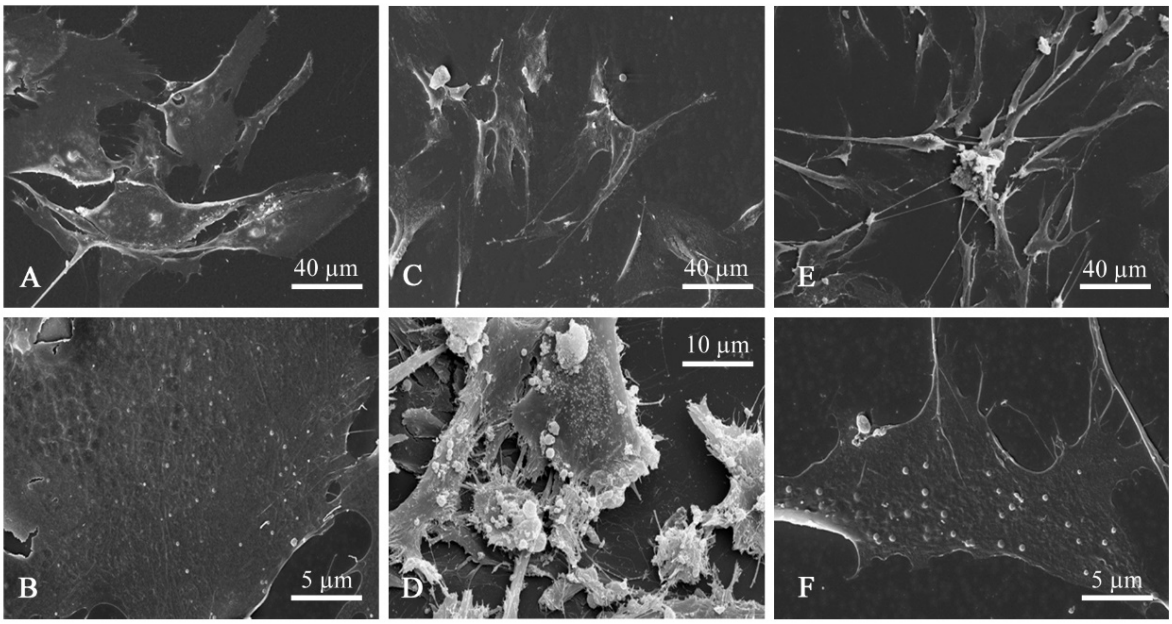

Figure 25. SEM micrographs of MRC-5 cells. (A, B) untreated; (C, D) treated with 2% w/w of the lyophilized SMEF; (E, F) treated with 5% w/w of the lyophilized SMEF for 6 h.

Based on the results of previous biological assays, 1% w/w of lyophilized SMEF was incorporated in an O/W emulsion (F1) to formulate a body cream, whose composition is shown in **Table 1**. Metals content of this formulation, determined by ICP-MS analysis, is shown in **Table 7**. The results evidenced a heavy metals content below limits provided by Italy, German Federal Government and Canada. In particular, As, Cd, Hg, Sb and Co were less than 0.05 mg/kg; Cr and Ni were less than 1 mg/kg.

Table 7. Metals content of emulsion containing lyophilized SMEF (1% w/w)

Metal	mg/kg	Limits as impurities in cosmetics (mg/kg)		
		Italy[(b)]	Germany[(a)]	Canada[(c)]
As	< 0.05	1	5	3
Cd	< 0.05	5	5	3
Hg	< 0.05	1	1	3
Pb	0.72 ± 0.01	20	20	10
Sb	< 0.05	10	10	5
Cr	0.51 ± 0.02	1	-	-
Co	< 0.05	5	-	-
Ni	0.50 ± 0.01	10	-	-
Al	6.11 ± 0.11	-	-	-
Cu	0.21 ± 0.01	-	-	-
Zn	5.95 ± 0.21	-	-	-
Fe	2.62 ± 0.05	-	-	-
Mn	0.52 ± 0.01	-	-	-
Sn	0.14 ± 0.01	-	-	-
Mo, Tl, Be,Ag, Bi, V	< 0.05	-	-	-

Metal content determined by ICP-MS in our experimental model, represented in comparison with limit content provided by some countries (Italy, Germany, Canada).

[a] BfR, Bundesinstitut für Risikobewertung. Kosmetische Mittel: BfR empfiehlt Schwermetallgehalte über Reinheitsanforderungen der Ausgangsstoffe zu regeln, Stellungnahme Nr. 025/2006 des BfR vom 05. April 2006.

[b] B. Bocca, A. Pino, A. Alimonti and G. Forte, Toxic metals contained in cosmetics: A status report, *Regul. Toxicol. Pharmacol.,* 2014, 68, 447-467.

[c] HC-SC, Health Canada-Santé Canada, 2012. Guidance on Heavy Metal Impurities in Cosmetics.

The pH value of F1 emulsion was weakly acidic (5.62 ± 0.02). Values regarding pH, appearance and phase separation were measured to assess physical and chemical stability during the storage period as reported in Materials and Methods section. F1 emulsions stored at 25°C±2°C with 60±5% R.H. did not show a significant change over time neither in pH nor in exterior aspect. F1 emulsions stored at 40°C±2°C with 60±5% R.H. for 6 months

showed a pH equal to 5.37 ± 0.02 and a minimal browning. Moreover, phase separation was not observed in any of samples. In addition, no significant changes in pH, phase separation and/or exterior aspect were observed in F1 samples with respect to base formulation (F0).

We also evaluated the moisturizing properties of both F0 and F1 emulsions *in vivo*. The results, reported in **Figure 26**, showed that F1 containing the lyophilized SMEF (1% w/w) determined an % increase of skin hydration (Group A:122,72%) with respect to F0 (Group B: 57,69%) after 7 days of body cream application and also with respect to day 0.

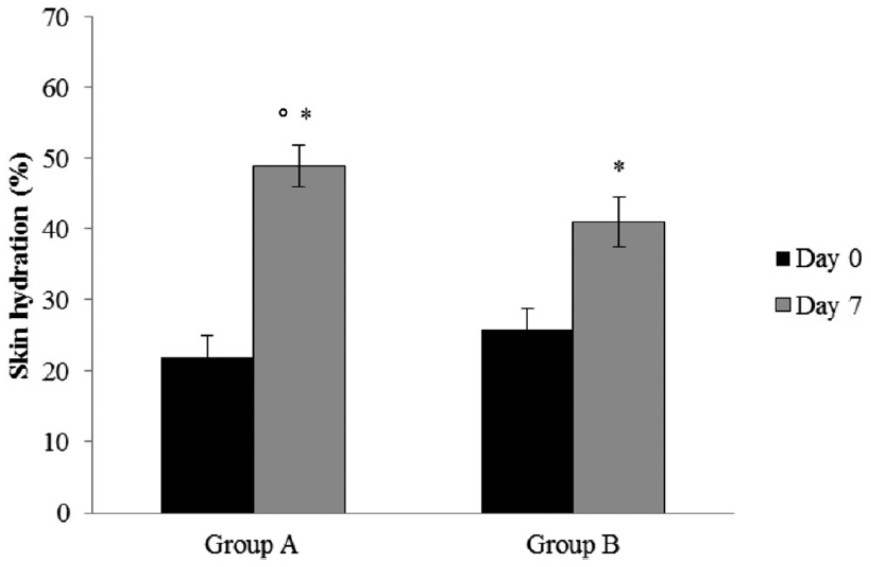

Figure 26. Skin hydration (%) evaluated by measuring the electrical impedance in volunteers before (day 0) and after (day 7) application, on an assigned area, of 20 mg of the emulsion containing 1% w/w of the lyophilized SMEF (group A) or the base emulsion (group B).
*Values significantly different vs. day 0 ($p < 0.05$). °Values significantly different vs. F0.

4.3 Studies for nutraceutical application of H-EF on human astrocytoma 1321N1 cells

Figure 27 reports the MTT assay data obtained on human astrocytoma cells treated for 24 and 48 hours with different concentrations of H-EF (50, 100 and 200 μM). As standard, as reported in Materials and Methods section, we chose HTyr.

The treatments with H-EF determined a drastic decrease in cell viability in a dose- and time-dependent manner. In contrast, HTyr 100 µM did not influence cell viability either after 24 and 48 hours of treatment. Taking into account these results, we decided to exclude, for the subsequent experimental phases, the highest concentration of H-EF (200 µM) because of its manifested toxicity.

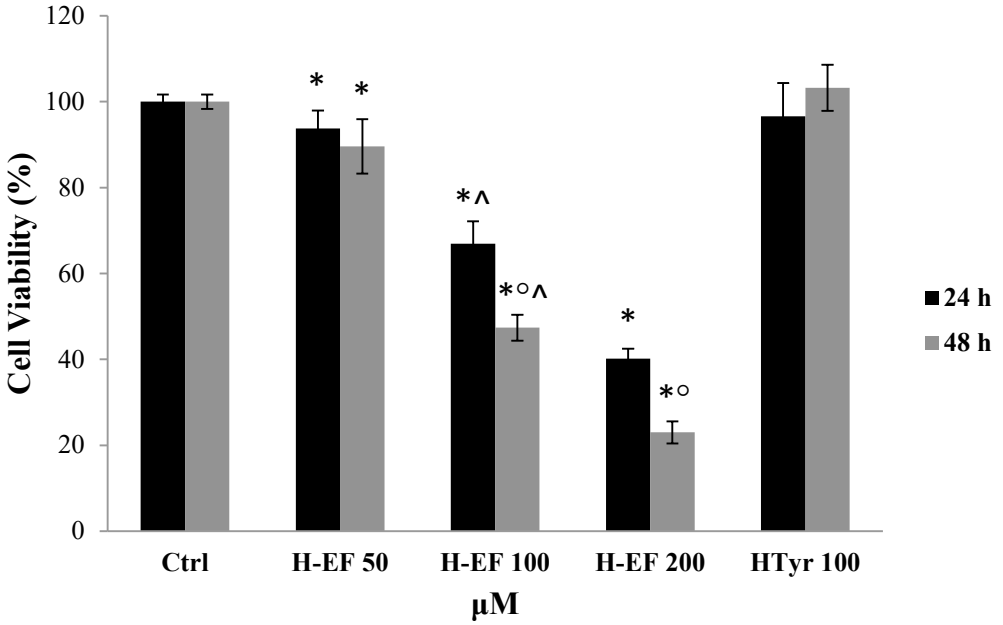

Figure 27. MTT assay performed on astrocytoma cells untreated and treated with different concentrations of H-EF (50, 100 and 200 µM) or HTyr (100 µM) for 24 and 48 hours. The results, expressed as the percentage of cell viability with respect to untreated control cells (Ctrl), are mean ± SD of three experiments each performed in triplicate. * $p < 0.05$ vs. control group; ° $p < 0.05$ vs. same treatment at 24h; ^ $p< 0.05$ vs. Htyr treatment at the same incubation time.

Figure 28 reports the results of Wound Healing assay performed on 1321N1 cells both untreated and treated with different concentrations of H-EF (50 and 100 µM) or HTyr (100 µM) for 24, 48 and 72 hours. As evidenced, H-EF significantly inhibited the cell migration capability in a dose- and time-dependent manner with respect to untreated control cells and HTyr-treated cells. **Figure 29** shows the images related to the data expressed in **Figure 28**.

These have been acquired by a phase-contrast microscope, either at the beginning of the assay and after 72 hours.

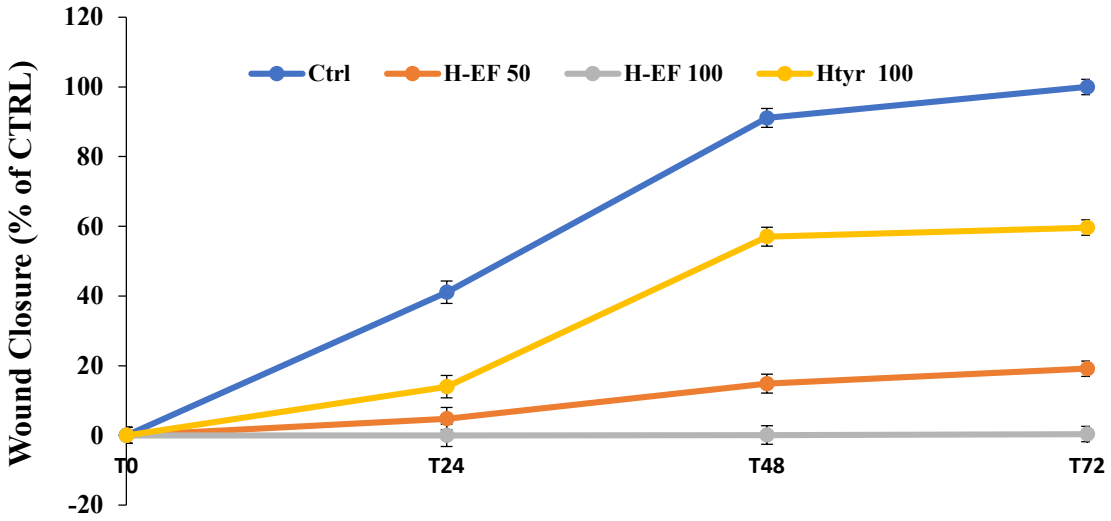

Figure 28. Wound Healing assay performed on 1321N1 cells untreated and treated with different concentrations of H-EF (50 and 100 µM) or HTyr (100 µM) for 24, 48 and 72 hours. The results are mean ± SD of three experiments each performed in triplicate.

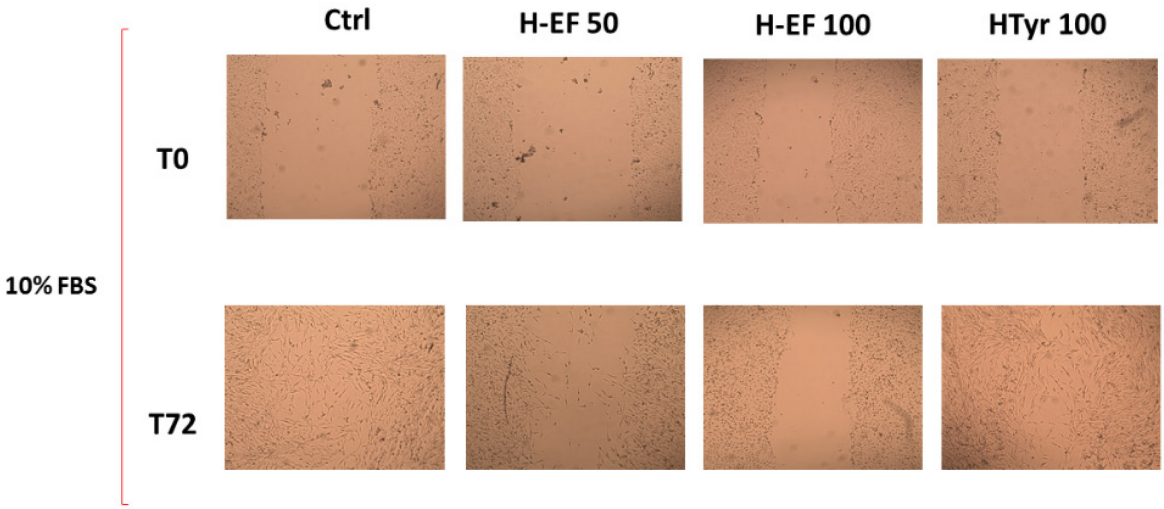

Figure 29. Images of Wound Healing assay performed on 1321N1 cells untreated and treated with different concentrations of H-EF (50 and 100 µM) or HTyr (100 µM). The images have been acquired by a phase-contrast microscope at the beginning of the assay and after 72 hours.

Table 8 represents the results of cell cycle analysis performed by flow cytometry on 1321N1 cells untreated and treated for 24 and 48 hours with different concentrations of H-EF (50 and 100 μM) or HTyr (100 μM). H-EF (50 and 100 μM) promoted the cell cycle arrest in G1 phase both after 24 and 48 hours of treatment. In contrast, HTyr 100 μM induced an arrest in S phase at 24 hours and in G1 phase at 48 hours.

Table 8. Cell cycle analysis performed by flow cytometry on 1321N1 cells untreated and treated with different concentrations of H-EF (50 and 100 μM) or HTyr (100 μM) for 24 and 48 hours.

	Cell cycle distribution (%)					
	24 h			**48 h**		
	G1	S	G2	G1	S	G2
Ctrl	37.44±1.57	45.33±2.09	17.24±0.98	43.21±1.22	35.23±1.45	21.55±2.88
H-EF 50	75.14±2.89*^	24.85±1.45*^	0.01±0.01*^	89.03±0.89*°	3.25±1.22*^°	7.72±1.14*°
H-EF 100	80.76±0.78*^	14.23±2.87*^	5.02±0.99*^	86.08±2.44*	13.92±3.23*^	0.01±0.01*^°
HTyr 100	26.24±2.66*	60.75±3.56*	13.02±2.44	87.97±1.98*°	6.83±0.76*°	5.20±1.12*°

The results are mean ± SD of three experiments each performed in triplicate. * $p < 0.05$ vs. control group; ° $p < 0.05$ vs. same treatment at 24h; ^ $p < 0.05$ vs. Htyr treatment at the same incubation time.

Figure 30 reports the results of LDH release assay performed on 1321N1 untreated and treated for 24 and 48 hours, either with H-EF or HTyr. H-EF increased the percentage of LDH release in a dose- and time-dependent manner with respect to untreated control cells. In addition, H-EF 100 μM significantly increased LDH release (%) with respect to HTyr-treated cells.

The DNA damage extent, evaluated by alkaline Comet assay, showed that both H-EF and HTyr were able to increase the damage only in a time-dependent manner (**Figure 31**).

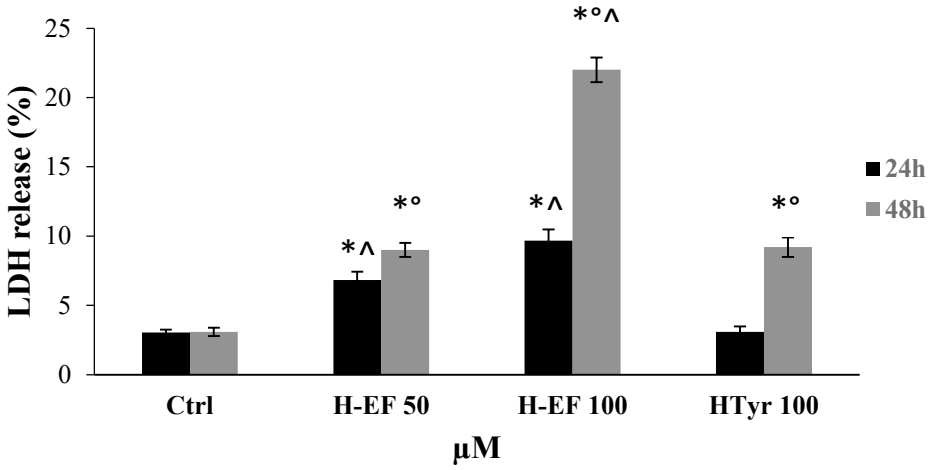

Figure 30. LDH release evaluated spectrophotometrically in the culture medium and in the cellular lysates at λ 340 nm by analizing NADH reduction. The assay was performed on 1321N1 cells untreated and treated with different concentrations of H-EF (50 and 100 µM) or HTyr (100 µM) for 24 and 48 hours. The results are expressed as LDH release (%). Values are mean ± SD of three experiments each performed in triplicate. * $p < 0.05$ vs. control group; ° $p < 0.05$ vs. same treatment at 24h; ^ $p< 0.05$ vs. HTyr treatment at the same incubation time.

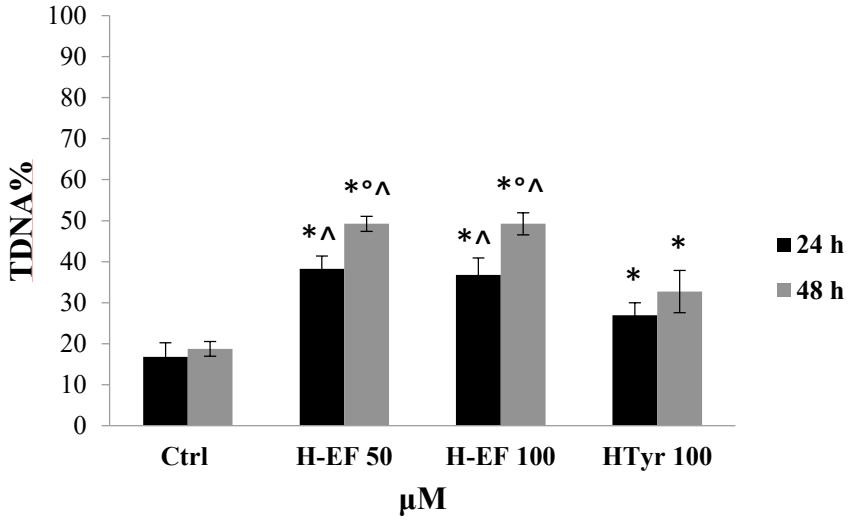

Figure 31. DNA damage evaluated by alkaline comet assay performed on 1321N1 cells untreated and treated with H-EF (50 and 100 µM) or HTyr (100 µM) for 24 and 48 hours. The results are expressed as the percentage of DNA present in the comet tail (%TDNA). Values are mean ± SD of three experiments each performed in triplicate. * $p < 0.05$ vs. control group; ° $p < 0.05$ vs. same treatment at 24h; ^ $p< 0.05$ vs. HTyr treatment at the same incubation time.

In order to elucidate the possible involvement of oxidative stress in treatment-induced damage, we examined ROS levels by DCFH-DA (**Figure 32**) and GSH levels by DTNB (**Figure 33**). As shown, H-EF 50 µM did not determine significant changes in ROS levels, conversely, only an increase in GSH levels after 48 hours of treatment. H-EF 100 µM determined a significant increase in ROS production with respect to untreated control cells and HTyr-treated cells both at 24 and 48 hours. Moreover, H-EF 100 µM determined an increase in GSH levels at 24 hours and a decrease at 48 hours. The treatment with HTyr 100 µM for 24 hours did not show any effect on redox status; in contrast, when it was added for 48 hours, ROS levels decreased and GSH levels increased with respect to untreated control cells.

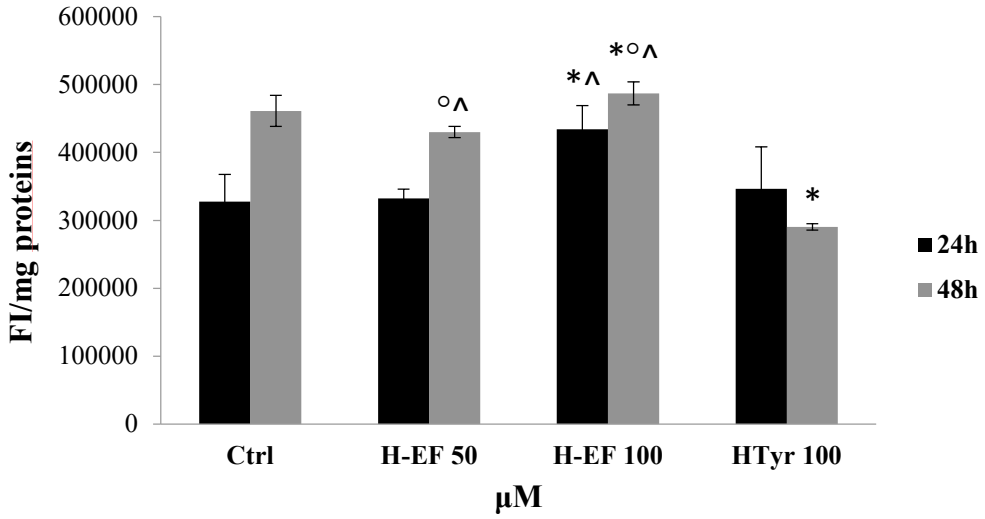

Figure 32. ROS levels measured spectrofluorimetrically in untreated and treated astrocytoma cells with different concentrations of H-EF (50 and 100 µM) or HTyr (100 µM) for 24 and 48 hours. The results were expressed as fluorescence intensity (FI) per mg proteins. Values are mean ± SD of three experiments each performed in triplicate. * $p < 0.05$ vs. control group; ° $p < 0.05$ vs. same treatment at 24h; ^ $p< 0.05$ vs. HTyr treatment at the same incubation time.

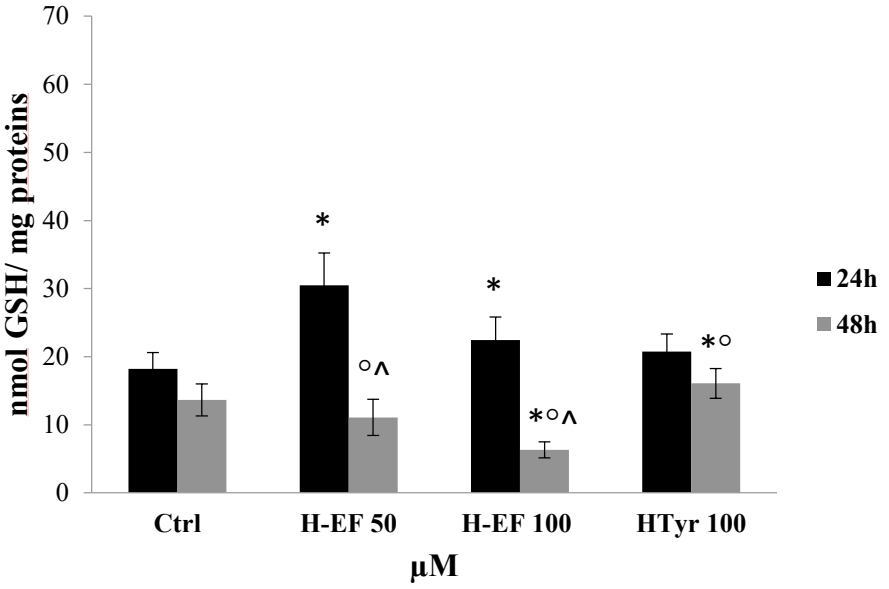

Figure 33. GSH levels measured on untreated and treated astrocytoma cells with different concentrations of H-EF (50 and 100 µM) or HTyr (100 µM) for 24 and 48 hours. The results were expressed as nmol GSH per mg proteins. Values are mean ± SD of three experiments each performed in triplicate. * $p < 0.05$ vs. control group; ° $p < 0.05$ vs. same treatment at 24h; ^ $p< 0.05$ vs. HTyr treatment at the same incubation time.

In **Figures 34** and **35** the results of Western Blot analysis are shown. We investigated the expression of p53, p21 and SIRT1 proteins. We observed that Htyr 100 µM increased p53 expression both at 24 and 48 hours, but it decreased the expression of p21 only at 24 hours; both concentrations of H-EF were able to decrease the expression of p53 and p21 with respect to untreated control cells (**Figure 34**).

Regarding the expression of SIRT1, H-EF 50 µM increased SIRT1 expression at 24 hours and decreased its expression only at 48 hours, H-EF 100 µM was able to decrease SIRT1 expression in a time-dependent manner. In contrast, HTyr 100 µM increased SIRT1 expression, especially at 24 hours (**Figure 35**).

In addition, **Figure 36** shows the sirtuins activity measured only on nuclear extracts.

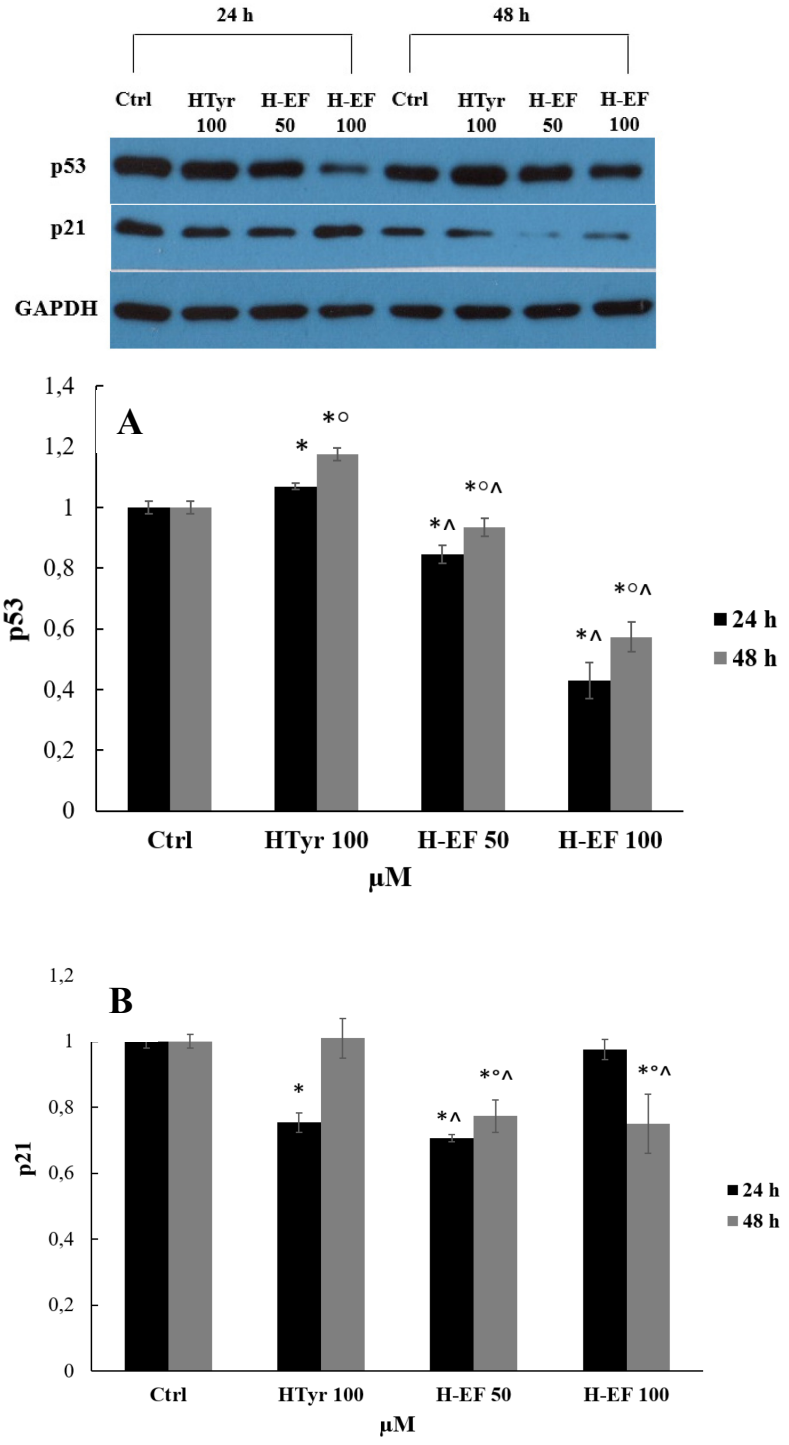

Figure 34. Expression of p53 (A) and p21 (B) in 1321N1 cells untreated and treated with different concentrations of H-EF (50 and 100 µM) or HTyr (100 µM) for 24 and 48 hours. GAPDH was used as loading control. Values are mean ± SD of three experiments each performed in triplicate. * $p < 0.05$ vs. control group; ° $p < 0.05$ vs. same treatment at 24h; ^ $p < 0.05$ vs. HTyr treatment at the same incubation time. Western immunoblotting images refer to one experiment.

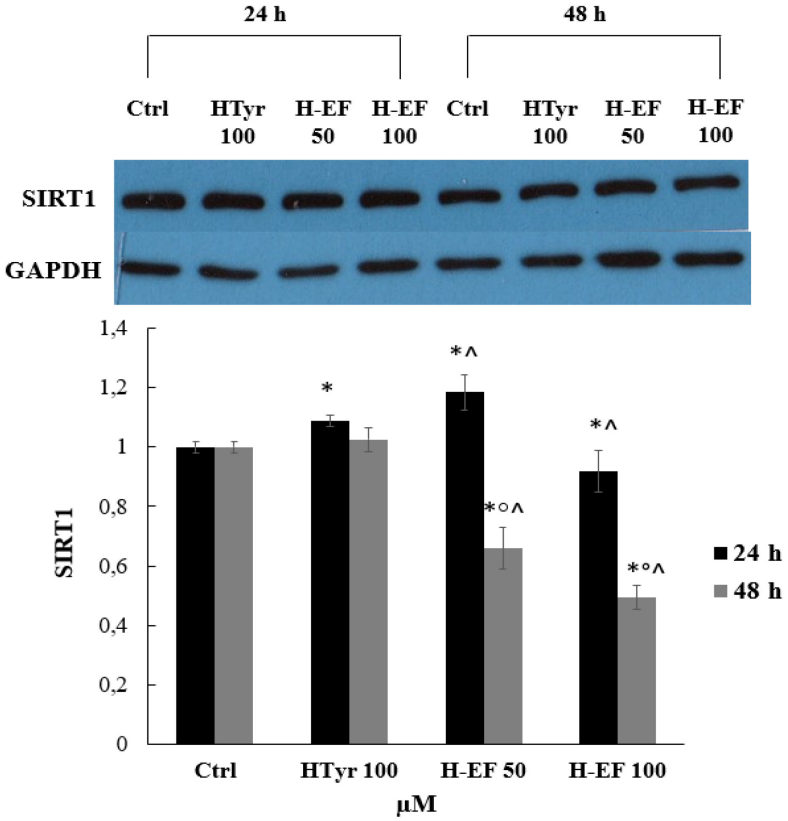

Figure 35. Expression of SIRT1 in 1321N1 cells untreated and treated with different concentrations of H-EF (50 and 100 µM) or HTyr (100 µM) for 24 and 48 hours. GAPDH was used as loading control. Values are mean ± SD of three experiments each performed in triplicate. * $p < 0.05$ vs. control group; ° $p < 0.05$ vs. same treatment at 24h; ^ $p< 0.05$ vs. HTyr treatment at the same incubation time. Western immunoblotting images refer to one experiment.

The preliminary results evidenced that H-EF 100 µM was able to decrease the nuclear sirtuins activity in a time-dependent manner; in contrast HTyr increased the activity only at 48 hours.

Figure 37 shows the preliminary results of global methylation analysis performed by Methy-sens Comet assay. The results evidenced that H-EF 100 µM induced DNA hypermethylation, while both H-EF 50 µM and HTyr 100 µM induced DNA methylation.

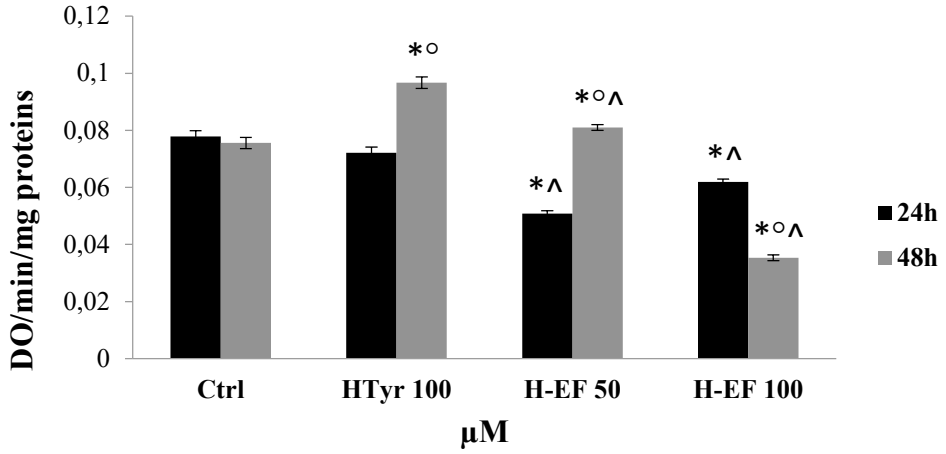

Figure 36. Sirtuins activity evaluated on nuclear extracts obtained from 1321N1 cells untreated and treated with different concentrations of H-EF (50 and 100 µM) or HTyr (100 µM) for 24 and 48 hours. The results were expressed as DO/min/mg proteins. Values are mean ± SD of three experiments each performed in triplicate. * $p < 0.05$ vs. control group; ° $p < 0.05$ vs. same treatment at 24h; ^ $p< 0.05$ vs. HTyr treatment at the same incubation time.

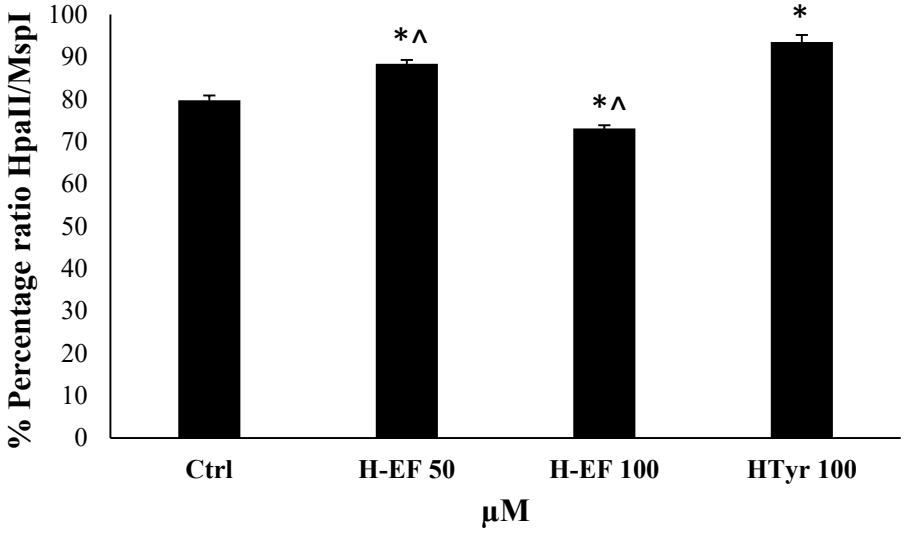

Figure 37. Global DNA methylation analysis performed by Methy-sens Comet assay on 1321N1 cells untreated and treated with different concentrations of H-EF (50 and 100 µM) or HTyr (100 µM) for 24 hours. The results were expressed as the percentage ratio HpaII/MspI. Values are mean ± SD of three experiments each performed in triplicate. * $p < 0.05$ vs. control group; ^ $p< 0.05$ vs. HTyr treatment at the same incubation time.

CHAPTER V

DISCUSSION

5.1 Chemical analysis of OMWW

OMWW produced during the processing of Cerasuola and Nocellara etnea, two very important Sicilian olive cultivars, were freshly collected in the middle-late of the milling period; since they originated from a three-phase continuous apparatus, samples contained solid residues which were eliminated by centrifugation and filtration. To reduce the formation of artifacts and to inhibit chemical modifications, samples were flash-freezed straight after collection and stored at -20 °C into airtight screw-capped tanks.

Initially, we performed a physicochemical characterization of both OMWW whose results (**Table 2)** showed that they had a mildly pH in according to values (pH 3-6) reported by Cardoso et al., 2011. In addition, both waters were characterized by high COD levels along with minerals, especially potassium (in the range 4.73-7.38 g/l), in accordance with literature data. OMWW are a complex matrix known for their very variable amounts of polyphenols ranging from 0.5 to 24 g/l (D'Antuono et al., 2014). However, most of literature data report the polyphenolic composition of OMWW extracts obtained through membrane filtration systems, adsorption/desorption processes or solvent extraction (Aggoun et al., 2016; D'Antuono et al., 2014; He et al., 2012) but this approach could modify the original quali-quantitative profile; for this reason, we evaluated the polyphenolic composition of untreated waters. The total phenolic contents of both OMWW are consistent with those commonly found in literature and concerning different cultivars. It is worth noting that Cerasuola-OMWW present a total polyphenolic and flavonoid content which is almost

double compared to Nocellara etnea-OMWW (**Table 3**). Polyphenolic characterization of OMWW was carried out by HPLC-DAD. Recording spectra at 280 nm allowed us to detect most of biophenols present in the matrix with acceptable intensity and signal to noise ratio. The chromatograms, shown in **Figure 18**, highlighted a quantitative rather than a qualitative difference in the polyphenolic profiles of Cerasuola-OMWW and Nocellara etnea-OMWW. The quantification of such complicated mixtures is a challenge; the concentration of the single biophenols in the samples was determined on the base of the corresponding peak area value related to a calibration curve obtained as depicted in the Materials and Methods section: hydroxytyrosol, tyrosol, caffeic acid, pyrocatechol, floretic acid, *p*-coumaric acid and *trans*-ferulic acid were identified and quantified as reported in **Table 3**.

Data showed that hydroxytyrosol and tyrosol are the main phenolic constituents of both OMWW according to several previous reported investigations (D'Antuono et al., 2014). However, the qualitative and quantitative profiles of the biophenolic content in OMWW from different sources change on a case-by-case basis. For instance, none of the principal biophenolic constituents found by Casa et al. (2003) in an Italian OMWW has been detected in the current analyzed samples. Furthermore, to underline the specificity of each biomass, we can observe that oleuropein, (the ester of elenolic acid and hydroxytyrosol) already reported as the most abundant polyphenol in OMWW by some authors (Visioli et al., 2002), is present only in small amounts (not quantifiable) in our samples; these differences in oleuropein concentrations are probably due to the different sampling period. In our case, olives were milled when mature and, at that time, most of oleuropein had already been metabolized into the corresponding phenolic and acidic precursors. As a support to this hypothesis, we found high amounts of hydroxytyrosol in both waters. In addition, gallic acid and vanillic acid often found in other OMWW (Aggoun et al., 2016; He et al., 2012), were not identified in any sample too.

Both OMWW were able to quench the DPPH radical in a dose-dependent manner and had a higher radical scavenging activity than the positive standard hydroxytyrosol, probably due to the synergistic effect of the other phenolic compounds (**Figure 19**). Polyphenols are a highly unstable species being involved in several biochemical and chemical reactions such as oxidation, condensation, polymerization and hydrolysis during food processing and storage. In this study, we evaluated the effects of storage time and temperatures on the specific OMWW polyphenolic compositions by measuring the variations of total phenolic, flavonoid and hydroxytyrosol contents. No significant change was observed with respect to total phenolic, flavonoid and hydroxytyrosol content in Cerasuola-OMWW and Nocellara etnea-OMWW samples stored at -20°C for 6 months (data not shown). On the other hand, the storage at 4°C and 25°C determined a decrease of total phenols and total flavonoids, especially in Nocellara etnea-OMWW, in a temperature- and time-dependent manner as shown in **Table 4**. Other authors evaluated the relative changes in the total phenols concentration in samples stored at different conditions, but they found only a very slight reduction ranging from 2% to 5% in samples stored at 4°C and 23°C under aerobic conditions (He et al., 2012). These results allowed us to establish the best storage conditions in order to minimize the loss of polyphenolic compounds, and imply the need of short storage periods in the olive mills collecting tanks (usually kept at room temperature) when a work-up of OMWW is expected.

5.2 Studies for cosmeceutical application of lyophilized SMEF

The second objective of my doctorate project was to evaluate the safety and the moisturizing properties of a sugars and minerals enriched fraction (SMEF), obtained from Cerasuola-OMWW, by *in vitro* and *in vivo* studies. We recovered SMEF through a green process, using for the first time the brominated polystyrenic resin PAD428 and water as the eluent.

The adopted resin was the result of a wide screening (not the object of this study and hereby not reported) of adsorbent materials both commercial and non-commercial, aiming at identifying a material able to retain phenolic compounds in an efficient way (and, consequently, allowing the production of a fraction completely devoid of phenols). The qualitative–quantitative sugar composition of the lyophilized SMEF by HPLC-ELSD analysis has been suggested as a good method to evaluate carbohydrates in different matrices such as plants, foods and drink products (Shanmugavelan et al., 2013). The results presented in **Table 5** evidenced that this fraction was rich in sugars (around 43%) in accordance with literature data (Dermeche et al., 2013). In contrast, we did not identify soluble polysaccharides, reported by other authors (Galanakis et al., 2010), probably because these compounds were highly diluted in OMWW or were hydrolyzed in their monosaccharide units due to the acidic pH of the sample. As a support to this hypothesis, we found high amounts of glucose, followed by mannose and fructose. With regard to the metal analysis performed by ICP-MS, **Table 6** shows that potassium was the most abundant mineral in accordance with literature data (Dermeche et al., 2013), whereas a very low concentration of heavy metals has been measured, making the fraction particularly suitable for applications in the cosmetic field.

Therefore, our interest was mainly in the evaluation of the possible cytotoxic effects elicited by the SMEF *in vitro.* The results on the SMEF-treated MRC-5 cells showed a toxic effect exhibited by the highest concentrations of the fraction in a time-dependent manner. In our opinion, this effect could be exerted by the increase in ROS production, considering the positive correlation between the viability and ROS level at 24 h. A similar result already reported by other authors (Lamers et al., 2011) leads us to affirm that the antioxidant capacity of the cells was, in turn, overcome by the over-production of ROS. The accumulation of oxidized intracellular macromolecules influenced the cell viability up until inducing cell

death (Acquaviva et al., 2016; Muscoli et al., 2002). Moreover, these observations have motivated us to examine the existence of a possible relationship among the other parameters we studied and the ROS levels. In our experimental model, we evidenced that the ROS level increase is correlated to the presence of positive apoptotic cells which arise in a time- and concentration-dependent manner (**Figure 22**). Furthermore, the observed increase in ROS level was related to DNA damage (**Figure 23**), demonstrating that this is one of the main contributors to cell death, particularly after 24 hours. In contrast, after 6 hours we observed some effects on DNA damage and apoptosis in cells treated with the highest concentration (2% and 5%) of the SMEF, without the influence on cell viability. These outcomes were also independent of the ROS levels as determined by the Pearson correlation test. We speculated that this early SMEF-induced DNA injury may result from the hypertonicity of the culture medium or a low DNA repair capability by glucose genetic control as suggested by Pang et al., 2012. We measured the osmolality of the culture medium and it increased from 0.278 Osm kg^{-1} for the basic medium up to 0.579 Osm kg^{-1} for the medium supplemented with 5% of the SMEF. Different studies (Lorenzi et al., 1986; Mavrogonatou and Kletsas, 2009; Tchounwou et al., 2014) have provided conflicting evidence about the relationship between DNA integrity and hyperosmolarity depending on the type of cell. It was recently established that hyperosmotic stress causes DNA breaks in mouse inner medullary collecting duct cells both *in vivo* and *in vitro* by stopping the cell cycle progression and the recruitment of DNA repair enzymes. In contrast, nucleus pulposus cells residing within a hyperosmotic environment clearly preserved their ability to sense and repair newly introduced DNA damage (Mavrogonatou and Kletsas, 2009). Lorenzi et al. (1986) reported that the presence of DNA damage in human endothelial cells exposed to high glucose as well as D-glucose induces cytotoxic, genotoxic, and apoptotic effects on MCF-7 cells (Tchounwou et al., 2014).

In order to verify the relationship between the altered intracellular homeostasis and the MRC-5 cytoarchitecture, we analyzed the cell morphology by SEM, well known for its ability to evidence, if present, typical apoptotic structures, such as blebs, apoptotic bodies and cell shrinkage (Burattini et al., 2009; Kavitha et al., 2017). Our data evidenced changes in the extramorphological features (**Figure 25**) exhibited by the lyophilized SMEF, proportional to the treatment concentration utilized in MRC-5 cells treated for 6 hours with the highest concentrations (2% and 5% w/w). By means of SEM analysis, in fact, we observed a shrunken cytoplasm and numerous blebs and ruffles on the cell surface. These morphological alterations, which are expression of the compromised cellular redox status with the involvement of DNA damage, may be produced by the possible formation of inter/intramolecular hydrogen bonds and/or by the presence of pores in the multiple membranes. These structural disarrangements are clear signs of apoptotic cell death supporting our results for the TUNEL test. In fact, cytoplasmic shrinkage is usually accompanied by nuclear events such as nuclear chromatin condensation/pyknosis and DNA fragmentation. Chromatin condensation leads to the nuclear matrix and lamina degradation followed by chromatin collapse, nucleus shrinkage and fragments of dense granular spheres with the consequent activation of enzymatic/proteic disarrangement leading to caspase mediated apoptosis (Coleman et al., 2001; Doonan and Cotter, 2008; Enari et al., 1998). It is plausible that hypertonicity causes the early effects on fibroblasts (DNA damage and morphological changes) and, after 24 hours, the outcomes may result from the combination of hypertonicity and ROS increase.

Taking into account the aforementioned *in vitro* results, an *in vivo* evaluation of the formulation supplemented with the SMEF was performed after assessing the physical stability. The analysis of the F1 emulsion stability revealed that the formulation was stable during the study. We observed a minimal change of color after 6 months at 40 °C and 60%

RH, probably because the SMEF undergoes aging following the oxidative and decomposition processes. Indeed, the SMEF was rich in sugars which - in the presence of nitrogen-containing compounds or amino acids in traces - reacted to produce melanoidin, a dark-colored substance which could be responsible for the color of the formulation (Bailey et al., 1995). Moreover, the determination of the metal content revealed that their concentrations in the samples were very low and below the limits set by some countries (Italy, Germany and Canada), as shown in **Table 7**. Metals in cosmetic products may undergo retention and act directly on the skin or be absorbed through the skin into blood, accumulate in the body and exert toxic effects in various organs. Several cases of systemic and topical effects related to the exposure to metals present in cosmetics have been reported (Borowska and Brzóska, 2015). Our data clearly showed that metals are not present in amounts creating a danger to human health in SMEF formulation, so this topical cream can be considered safe. Beyond safety and formulation stability, other desirable features of cosmeceutical agents are efficacy, novelty, patent protection, metabolism within the skin and inexpensive manufacture (Kadam Vaishali et al., 2013). Previous research has demonstrated that adequate hydration of the stratum corneum is an effective method to maintain healthy skin (Hoeksema et al., 2013). In our experimental design, skin hydration after 7 days following the daily application of the formulation was improved significantly, as shown by the increase of electrical impedance values (**Figure 26**). These data complied with those reported by other authors who have investigated different cosmetic formulations for their hydration properties (Fujioka et al., 2009; Wanitphakdeedecha et al., 2011). In particular, a formulation containing 0.1% of mucopolysaccharide polysulphate led to an improvement of skin hydration for at least 10 hours after a single application in women with dry skin (Wanitphakdeedecha et al., 2011). Our results indicated that the SMEF fraction obtained from OMWW could be developed as products for skin care and may also be added with

other bioactive compounds from different agro-food by-products possessing anti-aging, antioxidant, and anti-inflammatory activities, thus improving its cosmeceutical properties.

5.3 Studies for nutraceutical application of H-EF

The third objective of my doctorate project was to evaluate, *in vitro*, the chemotherapeutic activities exhibited by hydroxytyrosol-enriched fraction (H-EF) obtained from Cerasuola-OMWW through a green process, using activated charcoal and ethanol as already reported by our research group (Fava et al., 2017). The potential chemo-preventive activities of a polyphenol-rich purified extract from OMWW have been studied on different colon cancer cells by Bassani et al. (2016) and by Schaffer et al. (2010) on PC-12 cells by investigating the effects of Hytolive, a commercial HTyr-rich extract prepared from OMWW. We chose the human astrocytome cell line (1321N1) because, to our knowledge no data are present in literature regarding the potential anticancer effects of OMWW-polyphenolic extracts on these cell lines. As control, we used hydroxytyrosol commercial standard (HTyr).

In a preliminary way we have focused our research on the identification of the possible cytotoxic effect, measured as cellular viability (MTT assay), exerted on 1321N1 by different concentration of H-EF (50, 100 and 200 µM) and/or HTyr 100 µM, for 24 and 48 hours. All H-EF tested concentrations determined a dose- and time-dependent drastic decrease of cell viability, when compared with untreated control cells and HTyr-treated cells (**Figure 27**). On one hand, our data are in accordance with some literature data, evidencing the antiproliferative effects of a polyphenol-rich purified extract from OMWW on two human (HT-29, HCT-116) and one murine (CT-26) colon cancer cell lines (Bassani et al., 2016). On the other hand, these authors reported a similar antiproliferative effect exerted both by the extract and HTyr. However, we observed no significant changes in cell viability in HTyr-100 µM treated cells with respect to untreated control cells both at 24 and 48 hours as

reported by other authors also when the same molecule was used up to 200 μM (López de las Hazas et al., 2017).

These data evidenced that the observed effects should be considered in dependence of the employed cell type, paying attention to comparing results from different experimental plans. Considering the toxicity exerted, in our experimental model, by the highest concentration of H-EF, we have chosen to carry out the treatments for subsequent designed tests only with H-EF 50 and 100 μM concentrations.

To better define the antiproliferative effect elicited by our extract, we have also chosen to investigate its capability in preventing cell migration, by performing Wound Healing assay as reported in **Figure 28**. It is well known, in fact, that the migratory and invasive abilities of cancer cells are critical processes of the metastatic cascade (Albini et al., 2016). Our Wound Healing data, confirming antiproliferative effect elicited by H-EF, showed that the fraction significantly inhibited the migration capability of 1321N1 in a dose- and time-dependent manner with respect to untreated control cells and HTyr-treated cells, according to results obtained by Bassani et al., 2016. The greater effectiveness shown by H-EF than the standard, could be probably due, in our opinion, to the synergic effect elicited by other polyphenols present in H-EF.

Among the different effects elicited by hydroxytyrosol on cancer cell lines, a body of literature data has shown that, according with cellular types, it can arrest the cell cycle in different phases, affecting the expression of several cell-cycle-associated proteins. Our experimental contribution in this direction was expressed by performing both cell cycle analysis, on untreated and treated cells, by flow cytometry and the p53 and p21 proteins expression level by the immunoblotting. H-EF (50 and 100 μM) were able to arrest transition from G1 phase of cell cycle to S phase regulating commitment to cell division, both after 24 and 48 hours of treatment. In parallel, the expression of p21 and p53 has also decreased,

indicating the involvement of the effects elicited by H-EF treatment in genome stability and cell fate decision. In contrast, HTyr 100 μM induced an arrest in S phase at 24 hours and in G1 phase at 48 hours, as well as an increase in p53 expression at both incubation times and a decrease in p21 expression only at 24 hours (**Table 8** and **Figure 34**). Our results are in contrast with those reported by López de las Hazas et al. (2017) who have evidenced that HTyr 100 μM added to colon cancer cells for only 8 hours was able to arrest cell cycle in G1 phase. Also Zubair et al. (2017) have highlighted the ability of HTyr to arrest cell cycle in G1 phase in prostate cancer cells, alongside an increase the expression of p21, a small protein which can be induced by both p53-dependent and p53-independent mechanisms (Karimian et al., 2016). These data provide a proposal for future research to better investigate on regulatory mechanisms elicited by H-EF in different cancel cell lines in controlling cellular decision-making processes, changes in gene expression during cell cycle transitions and involved in transcriptional networks.

Several authors have reported that HTyr can induce later apoptosis and necrosis in different cancer cells such as colon cancer cells (Caco-2 and HT-29) and papillary and follicular thyroid cancer cells (López de las Hazas et al., 2017; Toteda et al., 2016). Our data are in accordance as we found that both extract and standard increased LDH release, a marker of necrotic death, in a dose- and time-dependent manner with respect to untreated control cells. However, H-EF 100 μM induced a greater LDH release with respect to HTyr-treated cells. It has been reported that necrosis generally occurs in response to severe changes in physiological conditions, including exposure to ROS (Elmore, 2007). Our results regarding LDH release can be related to the increase in intracellular ROS levels induced by H-EF treatment, seeming to act as pro-oxidant in 1321N1 cells (**Figure 32)**. The pro-oxidant activity of H-EF was also confirmed by the results regarding thiol groups determination which has evidenced the treatment with both concentrations of H-EF for 48 hours reduced

GSH levels (**Figure 33**), suggesting that the antioxidant system was not able to counteract the overproduction of ROS. Regarding HTyr elicited effects on redox state, we found a decrease in ROS levels at 48 hours, in contrast with literature data which have highlighted this biophenol as ROS increasing molecule in different cancer cell lines (Luo et al., 2013; Sun et al., 2014). This discrepancy may be explained by considering the different type of cell lines and the diverse concentration used.

Considering that cancer is a genetic and an epigenetic disease and that it is increasingly required to identify multiple biomarkers of exposure, of effect, of diagnosis and therapy, we investigated the effects elicited by H-EF on some epigenetic markers. During last decade, it has been demonstrated that alterations in epigenetic mechanisms may lead to several pathological conditions, including cancer (Kanwala and Gupta, 2012), but cell epigenetic status can be modulated by different natural compounds as polyphenols (Pan et al., 2013; Yang et al., 2014). DNA methylation is an epigenetic adaptation and disease-specific aberrant, a well-recognized hallmark of cancer and it is moving in defining personalized medicine.

In examining epigenetic modifications induced by hydroxytyrosol-enriched fraction from OMWW in our experimental model, we chose two approaches: 1) global methyloma analysis by Comet assay, 2) sirtuins expression/activity. The sirtuin family of histone deacetylases (SIRT 1-7) - enzymes which are dependent on NAD(+) for activity - has emerged as important regulators of different physio-pathological events, including cancer metabolism. Some members of this family are considered promising targets for cancer treatment due to their possible activation and inhibition by small molecule drugs and by some nutraceutical or phytotherapic compounds.

Among sirtuins, NAD^+-dependent deacetylases and mono-[ADP-ribosyl]transferases, we focused our attention on the expression of SIRT1, playing a dual role in cancer, operating as tumor suppressors or as an oncogenic factor.

The results of Western Blot analysis evidenced that H-EF 50 μM increased SIRT1 expression at 24 hours and decreased its expression only at 48 hours, H-EF 100 μM was able to decrease SIRT1 expression in a time-dependent manner. In contrast, HTyr 100 μM increased SIRT1 expression, especially at 24 hours (**Figure 35**). Literature data indicate that hydroxytyrosol (HTyr) regulates the autophagy of VAFs through SIRT1-mediated Akt/mTOR suppression (Wang et al., 2018), but no data on the effect of HTyr in human astrocytoma cells are present.

The difference we observed in modulation of activity and/or expression of sirtuins points out the pivotal function of these enzymes in genome maintenance and cell metabolism, and highlights current advances about the phenotypic consequences of defects in these critical regulators in tumorigenesis. However, on one hand, our data lead us to consider the existence of many questions to be addressed about the regulation and context-dependent functions of sirtuin, on the other hand, they clearly underline that sirtuins may be considered as a promising new avenue for cancer therapy (Jeong et al., 2015).

DNA methylation, essential for physiological processes, consists of the covalent addition of a methyl group from S-adenosyl-methionine (SAM) at the 5 position of the cytosine catalyzed by DNA methyltransferases (DNMTs). Certain dietary polyphenols, such as (-)-epigallocatechin 3-gallate (EGCG) from green tea and genistein from soybean, have been demonstrated to inhibit DNA methyltransferases (DNMT) *in vitro*. Mediterranean diet, extra virgin olive oil and its phenolic compounds, environmental/nutritional factor in epigenetics, are associated with a significant reduction of cancer risk, since many dysregulations of epigenetic pathways are present in cancer. Approaches pointing out prevention or reversal

of hypermethylation could be an effective approach for cancer treatment and/or prevencion. In our study, we analyzed the global methyloma by Methy-Sens Comet assay and evidenced DNA hypermethylation induced by H-EF 100 μM, while both H-EF 50 μM and HTyr 100 μM induced DNA hypomethylation (**Figure 37**). These results indicate that phenolic compounds, and in particular H-EF, may provide a new therapeutic avenue for treatment and/or prevention of human astrocytoma, also via epigenetic mechanism.

CHAPTER VI

CONCLUSIONS

Our results surely support the value of the green chemistry approach and encourage, as far as our experimental model concern, the use of OMWW (olive mill wastewater) from some Sicilian cultivars for the production of both H-EF (hydroxytyrosol-enriched fraction) and SMEF (sugars and minerals enriched fraction), to be considered for nutraceutical and cosmeceutical production respectively.

Our chemical characterization and preliminary assays on OMWW, evidenced the absence of dangerous metals, its ability in quenching the DPPH radical in a dose-dependent manner, its radical scavenging activity higher than hydroxytyrosol as positive standard, and its stability when stored at -20°C for 6 months.

In a second phase we recovered SMEF through a green process, by using for the first time - for this application and to our knowledge - the brominated polystyrenic resin PAD428 and water as the eluent and demonstrated, for the first time, the safe use of SMEF fraction in cosmeceutical field.

In fact, crossing our *in vitro* data (cytotoxicity, redox status, DNA damage and SEM determined cytoarchitetture analysis in MCR-5 cell lines) with *in vivo* results obtained by cooperating with Etnacosmesi company (Belpasso, Sicily) we established that the SMEF fraction obtained from OMWW could be developed as products for skin care. In addition it must be considered that SMEF cosmeceutical properties may also be improved if combined with other bioactive compounds from different agro-food by-products holding anti-aging, antioxidant, and anti-inflammatory activities.

Furthermore, with reference to H-EF, for the first time we evidenced and confirmed its chemotherapic properties in human astrocytoma cell lines, and underlined its potentiality as nutraceutical and/or dietary supplement. In fact, the H-EF inhibited proliferation and induced DNA necrotic damage probably modulated by alteration in ROS and GSH levels. These molecular events were associated with cell cycle arrest at G1 phase, down-regulation of p53, p21 and modulation, in dose-dependent way, of global DNA methylation and sirtuins activity/expression indicating the capability elicited by our extract in controlling genome stability and cell fate decision. Thus H-EF, particularly at highest concentrations, may be considered helpful in the prevention and/or integrative treatment of some tumor pathologies, as already reported by Bassani et al. (2016) but also in human astrocytoma, in which it was more effective than hydroxytyrosol (HTyr) used by us as standard, considering also epigenetic mechanism as a possible therapeutic avenue.

Still, considering the H-EF capability showed, in our experimental conditions, in both modulation of oxidative status and epigenetic activity, we think it could be largely suggested for applications in other different diseases, as cardiovascular, metabolic and neurodegenerative, not only as a nutraceutical having therapeutic target, but also as dietary supplement and/or compound to be managed for production of enriched, special and/or novel food.

However, although our results are very encouraging, it is clear that the possible therapeutic use of H-EF in humans requires additional studies on its biochemical/molecular mechanism and on possible synergic effect *in vivo*.

REFERENCES

Acquaviva et al., 2016. Effects of an extract of Celtis aetnensis (Tornab.) Strobl twigs on human colon cancer cell cultures. Oncol Rep., 2016, 36, 2298-2304

Aggoun M. et al. Olive mill wastewater microconstituents composition according to olive variety and extraction process. Food Chem, 2016, 209, 72-80

Albini A. et al. Extracellular Matrix Invasion in Metastases and Angiogenesis: Commentary on the Matrigel "Chemoinvasion Assay". Cancer Research, 2016, 76, 4595-4597

Alfano A. et al., 2018. Valorization of Olive Mill Wastewater by Membrane Processes to Recover Natural Antioxidant Compounds for Cosmeceutical and Nutraceutical Applications or Functional Foods. Antioxidants, 2018, 7(6). pii: E72. doi: 10.3390/antiox7060072

Aliakbarian B. et al. Antioxidant activity and biological evaluation of olive pomace extract. Nat Prod Res., 2012, 26(24):2280-2290

Alirezaie B. et al. Phenotypic and genomic analysis of serotype 3 Sabin poliovirus vaccine produced in MRC-5 cell substrate. J Med Virol, 2011, 83, 897-903

Allfrey V. G. et al. Acetylation and methylation of histones and their possible role in the regulation of RNA synthesis. Proc. Natl. Acad. Sci., 1964, 51, 786-794

Anastas P. and Eghbali N. Green Chemistry: Principles and Practice. Chem. Soc. Rev., 2010, 39, 301-312

Anastas P. T. and Warner J. C., in Green Chemistry: Theory and Practice, Oxford University Press, New York, 1998; I. Horvath and P. T. Anastas, Chem. Rev., 2007, 107, 2167.

Bahlis N. J. et al. Feasibility and correlates of arsenic trioxide combined with ascorbic acid-mediated depletion of intracellular glutathione for the treatment of relapsed/refractory multiple myeloma. Clin. Cancer Res., 2002, 8, 3658-3668

Bailey A. J. et al. Nonenzymatic glycation of fibrous collagen: reaction products of glucose and ribose, Biochem. J., 1995, 305, 385-390

Bassani B. et al. Potential chemopreventive activities of a polyphenol rich purified extract from olive mill wastewater on colon cancer cells. Journal of Functional Foods, 2016, 27, 236-248

BfR, Bundesinstitut für Risikobewertung. Kosmetische Mittel: BfR empfiehlt Schwermetallgehalte über Reinheitsanforderungen der Ausgangsstoffe zu regeln, Stellungnahme Nr. 025/2006 des BfR vom 05. April 2006.

Bianco A. et al., Analysis by liquid chromatography-tandem mass spectrometry of biophenolic compounds in olives and vegetation waters, Part I, J. Sep. Sci. 2003, 26, 409-416

Blois M.S. Antioxidant determinations by the use of a stable free radical. Nature, 1958, 181, 1199-1200

Bocca B. et al. Toxic metals contained in cosmetics: A status report, Regul. Toxicol. Pharmacol., 2014, 68, 447-467

Borowska S. and Brzóska M. M., Metals in cosmetics: implications for human health, J. Appl. Toxicol., 2015, 35, 551-572

Bosch-Presegué L. and Vaquero A. The Dual Role of Sirtuins in Cancer. Genes & Cancer, 2011, 2, 648-662

Bradford M.M. A rapid and sensitive method for the quantitation of microgram quantities of protein utilizing the principle of protein-dye binding. Anal Biochem., 1976, 72, 248-254

Burattini S. et al. Apoptotic DNA fragmentation can be revealed in situ: An ultrastructural approach, Microsc. Res. Tech., 2009, 72, 913-923

Cabrera F. et al. Land Treatment of Olive Oil Mill Wastewater, lnternational Biodeterioration & Biodegradation, 1996, 38, 215-225

Cardoso S.M. et al. Oleuropein/ligstroside isomers and their derivatives in Portuguese olive mill wastewaters. Food Chem, 2011, 129, 291-296

Casa R. et al. Reduction of the phenolic components in olive-mill wastewater by an enzymatic treatment and its impact on durum wheat (Triticum durum Desf.) germinability. Chemosphere, 2003, 50, 959-966

Cetrullo S. et al. Hydroxytyrosol prevents chondrocyte death under oxidative stress by inducing autophagy through sirtuin 1-dependent and -independent mechanisms. Biochim Biophys Acta., 2016, 1860, 1181-1191

Coleman M. L. et al. Membrane blebbing during apoptosis results from caspase-mediated activation of ROCK I, Nat. Cell Biol., 2001, 3, 339-345

Corona G. et al. Hydroxytyrosol inhibits the proliferation of human colon adenocarcinoma cells through inhibition of ERK1/2 and cyclin D1. Mol. Nutr. Food Res. 2009, 53, 897-903

Costa, F. F. et al. SATR-1 hypomethylation is a common and early event in breast cancer. Cancer Genet. Cytogenet., 2006, 165, 135-143

D'Adamo S. et al. Hydroxytyrosol modulates the levels of microRNA-9 and its target sirtuin-1 thereby counteracting oxidative stress-induced chondrocyte death. Osteoarthritis Cartilage, 2017, 25, 600-610

D'Antuono I. et al. Polyphenolic characterization of olive mill wastewaters, coming from Italian and Greek olive cultivars, after membrane technology. Food Res Int, 2014, 65, 301-310

Della Greca M. et al. Phytotoxicity of low-molecular-weight phenols from olive mill waste waters. Bull Environ Toxicol 2001, 67, 352-359

Denis M.C. et al. Apple peel polyphenols and their beneficial actions on oxidative stress and inflammation. PLoS One, 2013, 8, e53725

Dermeche S. et al. Olive mill wastes: Biochemical characterizations and valorization strategies, Process Biochem., 2013, 48, 1532-1552

Doonan F. and Cotter T. G. Morphological assessment of apoptosis, Methods, 2008, 44, 200-204

Dubois M. et al. , Colorimetric method for determination of sugars and related substances. Anal Chem, 1956, 28, 350-356

El-Abbassi A. et al. Phenolic profile and antioxidant activities of olive mill wastewater. Food Chem, 2012, 132, 406-412

Elmore S. Apoptosis: a review of programmed cell death. Toxicol Pathol., 2007, 35, 495-516

Enari M. et al. A caspase-activated DNase that degrades DNA during apoptosis, and its inhibitor ICAD, Nature, 1998, 391, 43-50

Fava G. et al. Hydroxytyrosol Recovery From Olive Mill Wastewater: Process Optimization and Development of a Pilot Plant, Clean: Soil, Air, Water, 2017, 45, 1600042

Ferri M. et al. Recovery of polyphenols from red grape pomace and assessment of their antioxidant and anti-cholesterol activities. N Biotechnol., 2016, 33, 338-344

Flynn T. C. et al. Dry Skin and Moisturizers, Clin. Dermatol., 2001, 19, 387-392

Folin O. Tyrosine and tryptophan determinations in proteins. J Biol Chem, 1927, 73, 672

Fujioka N. et al. Effects of various soap elements on skin. J. Anti-Aging Med., 2009, 6, 109-118.

Galanakis C et al. A study of the recovery of the dietary fibres from olive mill wastewater and the gelling ability of the soluble fibre fraction, LWT - Food Science and Technology, 2010, 43, 1009-1017

Ganta Vijay Chaitanya et al. PARP-1 cleavage fragments: signatures of cell-death proteases in neurodegeneration. Cell Commun Signal., 2010, 8, 31

Garbossa W. A. C. and. Maia Campos P. M. B. G. Euterpe oleracea, Matricaria chamomilla, and Camellia sinensis as promising ingredients for development of skin care formulations, Ind. Crops Prod., 2016, 83, 1-10

Goldsmith C.D. et al. The Olive Biophenols Oleuropein and Hydroxytyrosol Selectively Reduce Proliferation, Influence the Cell Cycle, and Induce Apoptosis in Pancreatic Cancer Cells. Int. J. Mol. Sci. 2018, 19, 1937; doi:10.3390/ijms19071937

Grasso S. et al. Hydroxytyrosol lipophilic analogues: enzymatic synthesis, radical scavenging activity and DNA oxidative damage protection. Bioorg Chem., 2007, 35, 137-152

Greger V. et al. Epigenetic changes may contribute to the formation and spontaneous regression of retinoblastoma. Hum. Genet, 1989, 83, 155-158

Hamden K. et al. Hypoglycemic and antioxidant effects of phenolic extracts and purified hydroxytyrosol from olive mill waste in vitro and in rats. Chem Biol Interact., 2009, 180, 421-432

HC-SC, Health Canada-Santé Canada, 2012. Guidance on Heavy Metal Impurities in Cosmetics.

He J. et al., Stability and antioxidant of purified olive mill wastewater extracts. Food Chem, 2012, 131, 1312-1321

Hoeksema H. et al. Scar management by means of occlusion and hydration: a comparative study of silicones versus a hydrating gel-cream, Burns, 2013, 39, 1437-1448

Hu T. et al. Hydroxytyrosol and Its Potential Therapeutic Effects. J. Agric. Food Chem. 2014, 62, 7, 1449-1455

Jacobs J.P. The status of human diploid cell strain MRC-5 as an approved substrate for the production of viral vaccines. J Biol Stand, 1976, 4, 97-99

Jeong S.M. et al. Sirtuins in Cancer: a Balancing Act between Genome Stability and Metabolism. Mol Cells., 2015, 38, 750-758

Kadam Vaishali S. et al. Cosmeceuticals an emerging concept: a comprehensive review, Int. J. Res. Pharm. Chem., 2013, 3, 308-316

Kanwala R. and Gupta S. Epigenetic modifications in cancer. Clin Genet, 2012, 81, 303-311

Karimian A. et al. Multiple functions of p21 in cell cycle, apoptosis and transcriptional regulation after DNA damage. DNA Repair, 2016, 42, 63-71

Kavitha N. et al. In situ morphological assessment of apoptosis induced by Phaleria macrocarpa (Boerl.) fruit ethyl acetate fraction (PMEAF) in MDA-MB-231 cells by microscopy observation. Biomed. Pharmacother., 2017, 87, 609-620

Kouzarides T. Chromatin modifications and their function. Cell, 2007, 128, 693-705

Kulis M. and Esteller M. DNA methylation and cancer. Adv Genet., 2010, 70, 27-56

Isaacs I. Perinatal (fetal and neonatal) astrocytoma: a review, Childs Nerv Syst., 2016, 32, 2085-2096

Laemmli U.K. Cleavage of structural proteins during the assembly of the head of bacteriophage T4. Nature, 1970, 227, 680-685

Lamers M. L. et al. High glucose-mediated oxidative stress impairs cell migration, PLoS One, 2011, 6, e22865

Li S. et al. Hydroxytyrosol inhibits cholangiocarcinoma tumor growth: an in vivo and in vitro study. Oncol Rep., 2014, 31, 145-152

Liou G-Y and Storz P. Reactive oxygen species in cancer. Free Radic Res. 2010, 44, 479-496

López de las Hazas et al. Hydroxytyrosol and the Colonic Metabolites Derived from Virgin Olive Oil Intake Induce Cell Cycle Arrest and Apoptosis in Colon Cancer Cells. J. Agric. Food Chem., 2017, 65, 6467-6476

Lorenzi M. et al. High glucose induces DNA damage in cultured human endothelial cells, J. Clin. Invest., 1986, 77, 322-325

Luo C. et al. Hydroxytyrosol promotes superoxide production and defects in autophagy leading to anti-proliferation and apoptosis on human prostate cancer cells. Curr Cancer Drug Targets, 2013, 13, 625-639

Malfa G. et al. Chemotherapeutic effects of resveratrol and its analogue 3,5,4′-trans-trimethoxystilbene on DU145 cells, Trends Cancer Res., 2010, 6, 45-54

Malfa G. et al. "Reactive" Response Evaluation of Primary Human Astrocytes After Methylmercury Exposure, J. Neurosci. Res., 2014, 92, 95-103

Marinova D. et al. Total phenolics and total flavonoids in bulgarian fruits and vegetables. J Univ Chem Technol Metall, 2005, 40, 255-260

Mavrogonatou E. and D. Kletsas. High osmolality activates the G1 and G2 cell cycle checkpoints and affects the DNA integrity of nucleus pulposus intervertebral disc cells triggering an enhanced DNA repair response, DNA Repair, 2009, 6, 930-943

Mirchamsy H. et al. Use of human diploid cell MRC-5, for production of measles and rubella virus vaccines. Dev Biol Stand, 1976, 37, 297-300

Muscoli C. et al. Ethanol-induced injury in rat primary cortical astrocytes involves oxidative stress: effect of idebenone, Neurosci. Lett., 2002, 329, 21-24

Obied H.K. et al. Effect of processing conditions, prestorage treatment, and storage conditions on the phenol content and antioxidant activity of olive mill waste. J Agr Food Chem, 2008, 56, 3925-3932

Pan M.H. et al. Epigenetic and disease targets by polyphenols. Curr Pharm Des., 2013, 19, 6156-6185

Pang et al. Altered expression of base excision repair genes in response to high glucose-induced oxidative stress in HepG2 hepatocytes, Med. Sci. Monit., 2012, 18, BR281-BR285

Paredes M.J. et al. Characteristics of soil after pollution with wastewaters from olive oil extraction plants. Chemosphere, 1987, 16, 1557-1564

Pontén J. and Macintyre H.E. Long term culture of normal and neoplastic human glia. Acta Pathol Microbiol Scand., 1968, 74, 465-486

Pu X. et al. Alkaline Comet Assay for Assessing DNA Damage in Individual Cells. Curr Protoc Toxicol., 2015, 65:3.12.1-11. doi: 10.1002/0471140856.tx0312s65.

Rana G. et al. Volatilisation of substances after spreading olive oil waste water on the soil in a Mediterranean environment. Agr Ecosys Environ, 2003, 96, 49-58

Rawlings A. V. and Harding C. R., Moisturization and skin barrier function, Dermatol. Ther., 2004, 17, 43-48

Rodrigues F. et al. Olive by-products: Challenge application in cosmetic industry. Ind. Crops Prod., 2015, 70, 116-124

Rodrigues F. et al. Application of Coffee Silverskin in cosmetic formulations: physical/antioxidant stability studies and cytotoxicity effects. Drug Dev Ind Pharm., 2016, 42, 99-106

Roig A. et al. An overview on olive mill wastes and their valorisation methods. Waste Manag. 2006, 26, 960-969

Rothe G. and Valet G. Flow Cytometric Analysis of Respiratory Burst Activity in Phagocytes With Hydroethidine and 2′,7′-Dichlorofluorescin, J. Leukocyte Biol., 1990, 47, 440-448

Routray W. and Orsat V. Chapter 8 - Plant By-Products and Food Industry Waste: A Source of Nutraceuticals and Biopolymers. Food Bioconversion, 2017, 279-315

Salerno L. et al. Antioxidant activity and phenolic content of microwave-assisted Solanum melongena extracts. Sci World J, 2014, 315473

Sarkar M. et al. Flow-Cytometric Analysis of Reactive Oxygen Species in Peripheral Blood Mononuclear Cells of Patients with Thyroid Dysfunction, Cytometry, Part B, 2005, 70, 20-23

Sawan C. and Herceg Z. Histone Modifications and Cancer. Advances in Genetics, 2010, 70, 57- 85

Schaffer S. et al. Cytoprotective effects of olive mill wastewater extract and its main constituent hydroxytyrosol in PC12 cells. Pharmacological Research, 2010, 62, 322-327

Schieber A. Side Streams of Plant Food Processing As a Source of Valuable Compounds: Selected Examples. Annu. Rev. Food Sci. Technol. 2017, 8, 5.1-5.16

Schmidt J.H. and Merciai S. (2014) Life cycle assessment of the global food consumption. In: Proceeding 9th international conference LCA of food. San Francisco, USA

Scoditti E. et al. Hydroxytyrosol suppresses MMP-9 and COX-2 activity and expression in activated human monocytes via PKCα and PKCβ1 inhibition. Atherosclerosis, 2014, 232, 17-24

Shanmugavelan P. et al. Evaluation of sugar content and composition in commonly consumed Korean vegetables, fruits, cereals, seed plants, and leaves by HPLC-ELSD, Carbohydr. Res., 2013, 380, 112-117

Sherr C.J. Cancer cell cycles. Science, 1996, 274, 1672.

Singleton V.L. and Rossi J.A. Colorimetry of total phenolics with phosphomolybdic–phosphotungstic acid reagents. Am J Enol Vitic, 1965, 16, 144

Springett K. and Merriman L. Assessment of the Skin and its Appendages, in Assessment of the Lower Limb, ed. M. M. Merrimen and R. T. Tollafield, Churchill Livingstone, London, 1995, 207.

Sugiyama Y.et al. Osmotic stress up-regulates aquaporin-3 gene expression in cultured human keratinocytes, Biochim. Biophys. Acta, 2001, 1522, 82-88

Sun L et al. Hydroxytyrosol induces apoptosis in human colon cancer cells through ROS generation. Food Funct., 2014, 5, 1909-1914

Tchounwou C. K. et al. D-Glucose-induced cytotoxic, genotoxic, and apoptotic effects on human breast adenocarcinoma (MCF-7) cells, J. Cancer Sci. Ther., 2014, 6, 156-160

Tejada S. et al. Cardioprotective Effects of the Polyphenol Hydroxytyrosol from Olive Oil. Curr Drug Targets, 2017, 18, 1477-1486

Toteda G. et al. High doses of hydroxytyrosol induce apoptosis in papillary and follicular thyroid cancer cells. J Endocrinol Invest, 2017, 40, 153-162

Trachootham D. et al. Targeting cancer cells by ROS-mediated mechanisms: a radical therapeutic approach? Nat Rev Drug Discov., 2009, 8, 579-591

Vaquero A. and Reinberg D. Sirtuins in biology and disease. Boca Raton, FL: CRC Press/Taylor & Francis; 2008.

Verdier-Sévrain S. and Bonté F., Skin hydration: a review on its molecular mechanisms, J. Cosmet. Dermatol., 2007, 6, 75-82

Vermeulen K. et al. The cell cycle: a review of regulation, deregulation and therapeutic targets in cancer. Cell Prolif., 2003, 36, 131-149

Visioli F. et al. Antioxidant and other biological activities of phenols from olives and olive oil. Med Res Rev, 2002, 22, 65-75

Wang W. et al. Hydroxytyrosol regulates the autophagy of vascular adventitial fibroblasts through the SIRT1-mediated signaling pathway. Canadian Journal of Physiology and Pharmacology, 2018, 96, 88-96

Wanitphakdeedecha R. et al. The effects of mucopolysaccharide polysulphate on hydration and elasticity of human skin, Dermatol. Res. Pract., 2011, 2011, 807906.

Wentzel J.F. et al. Assessing the DNA methylation status of single cells with the comet assay. Anal Biochem., 2010, 400, 190-194

Whang W. et al. Hydroxytyrosol regulates the autophagy of vascular adventitial fibroblasts through the SIRT1-mediated signaling pathway. Can J Physiol Pharmacol., 2018, 96, 88-96

Yang X. et al. Hydroxytyrosol Attenuates LPS-Induced Acute Lung Injury in Mice by Regulating Autophagy and Sirtuin Expression. Curr Mol Med., 2017, 17, 149-159

Zagklis D.P. et al. Purification of olive mill wastewater phenols through membrane filtration and resin adsorption/desorption. J Hazard Mater., 2015, 285, 69-76

Zhao B. et al. Hydroxytyrosol, a natural molecule from olive oil, suppresses the growth of human hepatocellular carcinoma cells via inactivating AKT and nuclear factor-kappa B pathways. Cancer Letters, 2014, 347, 79-87

Zhi LQ et al. Hydroxytyrosol inhibits the inflammatory response of osteoarthritis chondrocytes via SIRT6-mediated autophagy. Mol Med Rep., 2018, 17, 4035-4042

Zoric N. et al. Hydroxytyrosol expresses antifungal activity in vitro. Curr Drug Targets, 2013, 14, 992-998

Zubair H et al. Hydroxytyrosol Induces Apoptosis and Cell Cycle Arrest and Suppresses Multiple Oncogenic Signaling Pathways in Prostate Cancer Cells. Nutrition and Cancer, 2017, 69, 932-942

ADDITIONAL INFORMATIONS

Publications

1) Di Mauro M.D., Giardina R.C., Fava G., Mirabella E.F., Acquaviva R., Renis M., D'Antona N. *Polyphenolic profile and antioxidant activity of olive mill wastewater from two Sicilian olive cultivars: Cerasuola and Nocellara etnea.* Eur Food Res Technol 2017, 243, 1895-1903

2) Di Mauro M.D., Ferrito V., Scifo C., Renis M., Tomasello B. *Effectiveness of Natural Compounds on DNA Damage in Coris julis (Linneaus 1758) from a Polluted Marine Area.* Water Air Soil Pollut 2017, 228: 228. doi.org/10.1007/s11270-017-3415-4

3) Di Mauro M.D., Tomasello B., Giardina R.C., Dattilo S., Mazzei V., Sinatra F., Caruso M., D'Antona N., Renis M. *Sugar and mineral enriched fraction from olive mill wastewater for promising cosmeceutical application: characterization, in vitro and in vivo studies.* Food Funct. 2017, 8, 4713-4722

Conferences Partecipation

V International Plant Science Conference, 12-15 September 2018, Fisciano, Italy

- Acquaviva R., Di Giacomo C., Tomasello B., Malfa G.A., Tundis R., Loizzo M.R., Di Mauro M.D., Minafra L., Pisciotta P., Tringali R., Ragusa S., Cammarata F.P. *Effect of the Betula aetnensis Raf (Betulaceae) extract on breast cancer cells treated with androntheraphy* (Poster)

- Malfa G.A., Tomasello B., Di Mauro M.D., Acquaviva R., Di Giacomo C., Tundis R., Ragusa S., Renis M. *Anticancer properties of Myrtus communis L. (Myrtaceae) berries: preliminary studies on breast cancer cell line MCF-7* (Poster)

VIII Congresso Nazionale SINut, 15-16 June 2018, Bologna, Italy

- Di Mauro M.D., Tomasello B., Acquaviva R., D'Antona N., Renis M., Di Giacomo C. *Proprietà nutraceutiche di un estratto ricco in idrossitirosolo derivato da acque di vegetazione olearie su un modello cellulare di astrocitoma umano 132N1* (Oral comunication)

Convegno Internazionale Oncologia Integrata, 23-25 March 2018, Firenze, Italia

- Tomasello B., Di Mauro M.D., Acquaviva R., Liuzzo M.T., Liuzzo A., Sbisà E., Forte M.G., Bonucci M., Renis M. *Effects of sulphoraphane and myrosynase blend on human astrocytoma cells* (Poster)

49° Congresso Nazionale SIBioC, 16-18 October 2017, Firenze, Italia

- Tomasello B., Miraponte S., Santagati M., Di Mauro M.D., Malfa G., Fiumara A., Cinà D., Renis M., Di Giacomo C. *The world of ASD biomarkers: look for the needle in the haystack and discover new interesting indications for future researches* (Poster)

International Summer School on Natural Products, 3-7 July 2017, Naples, Italy

- Di Mauro M.D. *Chemotherapeutic effects of hydroxytyrosol-enriched fraction from olive mill wastewater on astrocytoma cells* (Flash Presentation)

11th World Congress on Polyphenols Applications, 20-21 June 2017, Vienna, Austria

- Di Mauro M.D., Tomasello B., Di Giacomo C., Caruso M., D'Antona N., Renis M. Chemotherapeutic effects of hydroxytyrosol-enriched fraction from olive mill wastewater on astrocytoma cells (Poster)

2nd Sino-Italian Symposium on Bioactive Natural Products, 24-25 November 2016, Naples, Italy

- Di Mauro M.D., Tomasello B., D'Antona N., Mazzei V., Sinatra F., Caruso M., Giardina R.C., Di Giacomo C., Renis M., Acquaviva R. *Sugars and minerals enriched fraction from Cerasuola olive mill wastewater: in vitro study for cosmetic applications* (Poster)
- Di Mauro M.D., Tomasello B., D'Antona N., Fava G., Giardina R.C., Di Giacomo C., Renis M., Acquaviva R. *Polyphenolic extract from olive mill wastewater: phytochemical characterization and antioxidant activity* (Poster)
- Acquaviva R., Tomasello B., Sorrenti V., Malfa G., Di Mauro M.D., Raffaele M., Ragusa S., Di Giacomo C. *Role of nitric oxide in experimental model of diabetic nephropathy: effects of Betula aetnensis Rafin extract* (Poster)

3° CONVEGNO ANNUALE ICB – CNR, 28-30 September 2016, Catania, Italy

- Di Mauro M.D., Tomasello B., Morrone R., Biondi D., Renis M., D'Antona N. *Recovery of high-added-value compounds from olive mill wastewater for cosmetic and ophthalmic applications* (Oral presentation)

Visiting PhD Student

I was a visitor PhD student in the Laboratory of Molecular Bases of Ageing at Nencki Institute of Experimental Biology (Warsaw, Poland) between June 21st and June 29th 2018. During my stay I performed the analyses (Western Blot) of sirtuins levels.

Reviewer Activity

I have reviewed five papers for the following MDPI journals in 2018: Molecules and Nutrients.

Tutoring Activity

- Tutor for Biochemistry at Department of Drug Sciences-University of Catania
- Tutor for Advanced Molecular Biology at Department of Biomedical and Biotechnological Sciences-University of Catania
- Tutor for Anatomy at Department of Drug Sciences-University of Catania
- Tutor for General Chemistry at Department of Drug Sciences-University of Catania
- Tutor for Organic Chemistry at Department of Drug Sciences-University of Catania

ACKNOWLEDGMENTS

I would like to thank Prof. Massimo Libra and Ferdinando Nicoletti for the opportunity to attend the PhD course in Basic and Applied Biomedical Sciences.

Then, I would like to thank Prof. Marcella Renis, my supervisor, and Dr Nicola D'Antona and Dr Barbara Tomasello, for the precious help they gave me during these three years.

I would like to thank all other collegues of Biochemistry Section and Department of Drug Science of University, especially Prof. Rosaria Acquaviva, Prof. Claudia Di Giacomo, Dr Giuseppe Malfa, Prof. Carmelo Puglia and Dr Rosa Santangelo.

I would like to thank Dr Anna Bielak-Zmijewska and Dr Wioleta Grabowska for their help to perform Western Blot analysis.

I would like to thank Prof. Lucia Domenica Del Sarto for proofreading my PhD thesis.

Finally I would like to thank all my family for its support.